International Journal of Nanomedicine

Dovepress
open access to scientific and medical research

Open Access Full Text Article

ORIGINAL RESEARCH

Accumulation of Iron Oxide-Based Contrast Agents in Rabbit Atherosclerotic Plaques in Relation to Plaque Age and Vulnerability Features

Alexander Sekita[1], Harald Unterweger[1], Sonja Berg[1], Sabine Ohlmeyer[2], Tobias Bäuerle[3], Kang H Zheng[4], Bram F Coolen[5], Aart J Nederveen[6], Claudia Cabella[7], Silvia Rossi[7], Erik SG Stroes[4], Christoph Alexiou[1], Stefan Lyer[1,*], Iwona Cicha[1,*]

[1]ENT-Department, Section of Experimental Oncology Und Nanomedicine (SEON), Else Kröner-Fresenius-Stiftung-Professorship, Universitätsklinikum Erlangen, Erlangen, Germany; [2]Institute of Radiology, Universitätsklinikum Erlangen, Erlangen, Germany; [3]Preclinical Imaging Platform Erlangen (PIPE), Universitätsklinikum Erlangen, Erlangen, Germany; [4]Department of Vascular Medicine, Amsterdam University Medical Center, University of Amsterdam, Amsterdam, the Netherlands; [5]Department of Biomedical Engineering and Physics, Amsterdam University Medical Center, University of Amsterdam, Amsterdam, the Netherlands; [6]Department of Radiology and Nuclear Medicine, Amsterdam University Medical Center, University of Amsterdam, Amsterdam, the Netherlands; [7]Bracco Imaging SpA, Centro Ricerche Bracco, Colleretto Giacosa, Turin, Italy

*These authors contributed equally to this work

Correspondence: Iwona Cicha, Universitätsklinikum Erlangen, Glückstr, 10a, Erlangen, 91054, Germany, Tel +49 9131 85 43953, Fax +49 9131 85 34828, Email Iwona.Cicha@uk-erlangen.de

Purpose: In this study, a detailed characterization of a rabbit model of atherosclerosis was performed to assess the optimal time frame for evaluating plaque vulnerability using superparamagnetic iron oxide nanoparticle (SPION)-enhanced magnetic resonance imaging (MRI).

Methods: The progression of atherosclerosis induced by ballooning and a high-cholesterol diet was monitored using angiography, and the resulting plaques were characterized using immunohistochemistry and histology. Morphometric analyses were performed to evaluate plaque size and vulnerability features. The accumulation of SPIONs (novel dextran-coated SPION^{Dex} and ferumoxytol) in atherosclerotic plaques was investigated by histology and MRI and correlated with plaque age and vulnerability. Toxicity of SPION^{Dex} was evaluated in rats.

Results: Weak positive correlations were detected between plaque age and intima thickness, and total macrophage load. A strong negative correlation was observed between the minimum fibrous cap thickness and plaque age as well as the mean macrophage load. The accumulation of SPION in the atherosclerotic plaques was detected by MRI 24 h after administration and was subsequently confirmed by Prussian blue staining of histological specimens. Positive correlations between Prussian blue signal in atherosclerotic plaques, plaque age, and macrophage load were detected. Very little iron was observed in the histological sections of the heart and kidney, whereas strong staining of SPION^{Dex} and ferumoxytol was detected in the spleen and liver. In contrast to ferumoxytol, SPION^{Dex} administration in rabbits was well tolerated without inducing hypersensitivity. The maximum tolerated dose in rat model was higher than 100 mg Fe/kg.

Conclusion: Older atherosclerotic plaques with vulnerable features in rabbits are a useful tool for investigating iron oxide-based contrast agents for MRI. Based on the experimental data, SPION^{Dex} particles constitute a promising candidate for further clinical translation as a safe formulation that offers the possibility of repeated administration free from the risks associated with other types of magnetic contrast agents.

Keywords: atherosclerosis, plaque vulnerability, rabbit model, macrophages, histology, tissue iron, SPION-enhanced MRI

Introduction

Despite steady developments in anatomical and functional imaging techniques, > 50% of culprit atherosclerotic plaques are still identified in the acute clinical setting when they manifest as myocardial infarction, sudden death or stroke.[1] As decision making in patients with atherosclerotic cardiovascular disease (CVD) currently relies on the measurement of

Received: 14 July 2023
Accepted: 14 December 2023
Published: 20 February 2024

stenosis degree, new approaches must be developed to reliably assess plaque rupture risk and thus reduce the risk of life-threatening cardiovascular events. Early detection of plaques prone to instability using existing imaging modalities in clinical settings could greatly facilitate targeted therapy to inhibit disease progression and prevent acute ischemic events.

Magnetic resonance imaging (MRI), a non-ionizing modality characterized by good spatial resolution and soft tissue contrast,[2] is considered a suitable technique for detecting and characterizing cardiovascular disorders upon the application of appropriate contrast agents. Currently used gadolinium-based contrast agents (GBCA) have good imaging properties as bright contrast agents and allow microvascular permeability evaluation in dynamic contrast-enhanced (DCE)-MRI,[3] but their use poses a risk to renally impaired patients.[4,5] Deposition of gadolinium in the central nervous system, which can also affect patients with normal renal function, may trigger neurological disorders.[6,7] The new generation of GBCA remains the predominant diagnostic tool for patients requiring contrast-enhanced MRI, and efforts are ongoing to design and synthesize more stable gadolinium chelators to further reduce gadolinium toxicity.[8–10] In parallel, superparamagnetic iron oxide nanoparticle (SPION)-based contrast agents could act as alternatives, but currently, no particles are approved for this application in Europe. Three different formulations (including ferumoxide (Feridex®/Endorem®), ferumoxtran-10 (Combidex®/Sinerem®), and ferucarbotran (Resovist®)) have been previously approved as intravascular contrast agent for MRI. Although ferumoxide was mainly applied for in vivo tracking of labelled stem cells in rodents,[11,12] multiple clinical studies have confirmed the utility of ferumoxtran-10 for imaging of cardiovascular pathologies[13–18] and its safety upon repeated administration.[19]

The particular suitability of ferumoxtran-10 for cardiovascular imaging was related to its clinical safety (only minor side effects were reported in the majority of cases, and no clinically relevant cardiac adverse events were observed)[20] and good pharmacokinetic properties, as their small hydrodynamic diameter (20–40 nm) allows for an extended circulation half-life (up to 24 h),[21] and thus, their widespread distribution in tissues, including infarcted myocardium or atherosclerotic plaques. Ferumoxtran-10, intended for diagnostic MRI of lymph nodes in pelvic cancers, was withdrawn from the market in 2008, following the withdrawal of the application for its marketing authorization due to insufficient demonstration of diagnostic benefits. As an off-label solution, the intravenous iron supplementation product, ferumoxytol (Feraheme®/Rienso®, 17–30 nm), which is currently only indicated for therapy of iron deficiency anemia in patients with chronic renal failure, was used as a contrast agent to characterize myocardial infarcts[22–25] and carotid plaques,[26,27] to monitor aneurysm progression,[28] and evaluate the utility of contrast-enhanced MRI for the assessment of atherosclerotic plaque permeability in patients with peripheral artery disease.[3] However, owing to its complement-activating properties,[29] ferumoxytol poses a serious risk of potentially fatal anaphylactic reactions. This limits its off-label use for imaging and underscores the urgent need for T_2 and T_2* contrast agents that are not only technically feasible in terms of imaging and pharmacokinetic properties, but also possess a much safer clinical profile.

Since the respective contrast agents are administered intravenously, their stability in the blood, low cytotoxicity, and non-immunogenicity are indispensable.[30] In our previous studies,[31,32] we described a novel superparamagnetic iron oxide nanoparticle (SPION)-based contrast agent characterized by good size tunability, imaging properties, and remarkable storage stability. SPION^{Dex} particles were designed and optimized to fulfill multiple feasibility and safety criteria, including 30 nm size to ensure long circulation time and enable plaque accumulation, crosslinked dextran shell to enhance colloidal stability and prevent complement activation, and irregular shape with a large aspect ratio to reduce immunogenicity. These characteristics, together with outstanding in vivo safety[29] set SPION^{Dex} particles from other injectable iron-oxide-based agents. We then addressed the problem of a suitable atherosclerosis model within the framework of contrast agent development. Iron oxide-based agents (mainly ferumoxtran-10 and ferumoxytol) have been previously tested in preclinical mouse[33] and rabbit models to detect atherosclerotic lesions,[34] monitor plaque progression in hyperlipidemic animals,[35] or to detect plaque rupture and healing using MRI.[36] However, while murine models of atherosclerosis are useful tools in gene knock-out studies or SPION-based, plaque targeting drug-delivery system development,[37,38] in vivo imaging of atherosclerosis in mice is problematic because of the small size of the vessels and the characteristics of the lesions, which are very different from those of humans. Therefore, we focused on a rabbit model of advanced atherosclerosis induced by balloon injury to the abdominal aorta and a high-cholesterol diet, which was previously used for iron oxide-enhanced atherosclerotic plaque imaging, albeit with considerable limitations.[39] Aiming at the optimization of this model for the detection of plaque vulnerability features, we investigated the progress of lesions with respect to time, in order to frame suitable conditions for SPION-based imaging in future studies. Further, we aimed to evaluate the accumulation of the new formulation, dextran-coated SPION^{Dex} in rabbit atherosclerotic plaques for the first time and compare it with reference nanoparticles, ferumoxytol.

The longitudinal design of this study enabled us to investigate the potential correlations between SPION accumulation and plaque vulnerability features and plaque age.

Materials and Methods

Reagents and Antibodies

Iron (III) chloride hexahydrate, dextran T40 (Mw = 40 kDa), and epichlorohydrin (ECH) were purchased from Sigma-Aldrich (Munich, Germany). Iron (II) chloride tetrahydrate was obtained from Merck (Darmstadt, Germany). NaOH, HCl (25%), NH_3 (25%), and nitric acid (65%w/w) were purchased from Roth (Karlsruhe, Germany). The reagents used for nanoparticle synthesis were of pharmaceutical (Ph. Eur) or highly pure (⩾99%) grade.

Sodium heparin was obtained from Braun (Melsungen, Germany). Trichrome staining reagents (acid fuchsine, acridine orange, 1% molybdophosphoric acid, and light green) and hematoxylin (Dako, Hamburg, Germany) were purchased from Merck. Fast Red staining was performed using Roth. Mouse monoclonal antibodies against rabbit macrophages (clone RAM-11) were obtained from Dako and mouse monoclonal anti-CD31 antibody (Clone JC/70A) from Novus Biologicals (Bio-Techne GmbH, Wiesbaden, Germany). Mouse monoclonal antibody against smooth muscle actin (clone 1A4 (asm1), Neobiotechnologies Inc, UnionCity, CA, USA) was purchased from antibodies-online GmbH, Aachen, Germany,

Particles

Ferumoxytol (Feraheme®) was purchased from AMAG Pharmaceuticals, Inc. (Waltham, MA, USA). Dextran-coated SPIONs ($SPION^{Dex}$) were synthesized using a cold gelation method as previously reported[31] and are briefly described below. First, 150 mM iron in the form of $FeCl_3$ and $FeCl_2$ was dissolved in a 10 wt% dextran solution, followed by cooling in an ice bath. Particle formation was initiated by adding ice-cooled ammonia at 25 vol%. Subsequently, the particles were heated to 75 °C and maintained at this temperature for 30 min, followed by cooling to the room temperature. The resulting particles were purified using dialysis and ultrafiltration.

Subsequently, the dextran layer was cross-linked with ECH with stirring to ensure enhanced particle stability. After cross-linking, purification, dialysis, and ultrafiltration of the particles, a colloidally stable particle suspension was obtained. Subsequently, the produced $SPION^{Dex}$ was sterile filtered using 0.22 µm syringe filters and stored at 4 °C until further use.

Particle Characterization

The hydrodynamic size of SPIONs was measured with a Malvern Nano ZS device (Malvern Panalytical, United Kingdom) using dynamic light scattering in the backscattered mode. An atomic emission spectroscopy device (MP-4200, Agilent Technologies, USA) was used to determine the iron concentration in the samples. For this purpose, particles were dissolved in nitric acid and cooked at 95 °C. After cooling, the samples were diluted with water and the iron concentration was measured with AES. The magnetic properties of the particles were evaluated by measuring the volume susceptibility of 1 mg Fe/mL in aqueous dispersion using an MS3/MS2G magnetic susceptibility device (Bartington, United Kingdom). Further detailed characterization of the $SPION^{Dex}$ was reported previously.[29,31,32]

Rabbit Model of Atherosclerosis

A rabbit model of balloon injury and atherogenic diet was used to induce atherosclerotic plaque development in the abdominal aorta. The study protocol was approved by the responsible authority (Regierung von Unterfranken in Würzburg, permission RUF-55.2.2–2532-2-549-12) implementing the German Animal Welfare Act. Animal housing and care conformed to Directive 2010/63/EU.

Eleven New Zealand white rabbits (weight 3.0–4.0 kg; age, 3–4 months; Charles River, France) were included in this study. The experimental setup is illustrated in Figure 1. Before surgery, all animals received an intramuscular injection of ketamine (50 mg/kg) and xylazine (5 mg/kg) to induce general anesthesia, which was subsequently maintained by intravenous administration of a 1:4 dilution of ketamine and xylazine in Ringer's solution. Prior to the ballooning

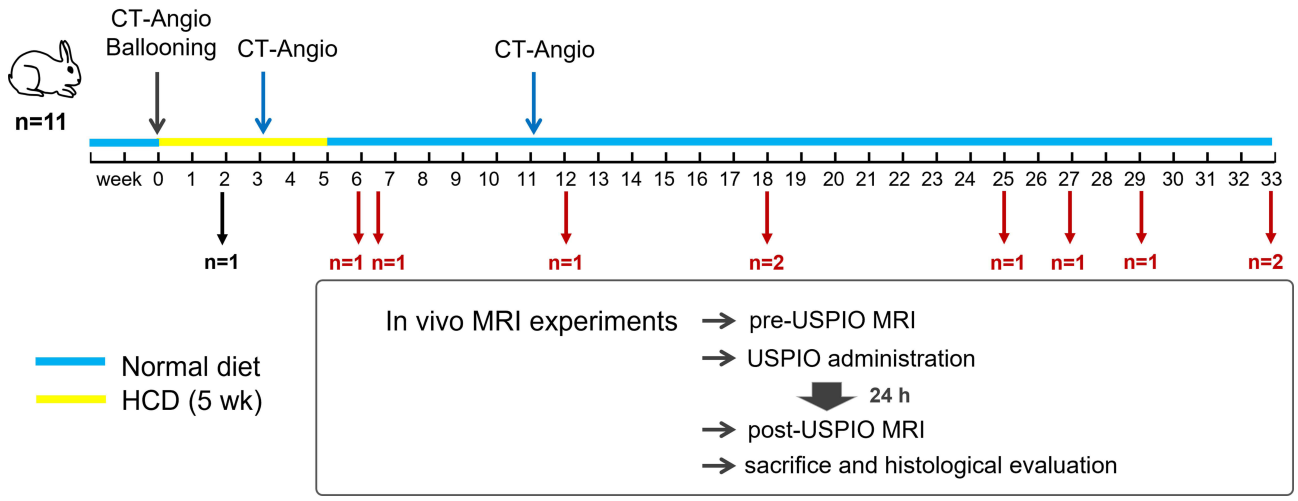

Figure 1 Schematic presentation of the experimental set-up indicating the duration of HCD and normal chow for individual animals, as well as the time of CT-angiography control and MRI imaging.
Notes: The arrows under the timeline indicate the endpoint of the experiment for the individual animals, with black arrow indicating one animal that was excluded from the study after refusing HCD.
Abbreviations: CT, computed tomography; HCD, high-cholesterol diet; MRI, magnetic resonance imaging; SPION, superparamagnetic iron oxide nanoparticles.

procedure, 3D angiographic images of the abdominal aorta were acquired using a Siemens Artis zee floor® computed tomography (CT)-angiography system (Siemens, Forchheim, Germany). For contrast enhancement, an iodine-based contrast agent (Imeron® 350, Bracco Imaging Deutschland GmbH, Konstanz, Germany) was administered via the ear vein. Subsequently, the left common carotid artery was exposed through a midline neck incision and a 4-French sheath was inserted. A 4-French catheter was then advanced into the descending aorta under angiographic control, followed by balloon injury to the lower abdominal aorta. Ballooning was performed manually without a pressure-controlling device. For better visualization during the procedure and to ensure stability of the inflated balloon, the catheter was filled with iodine-containing water. To injure the vessel wall, the balloon was positioned at the distal point of the injury area, near the bifurcation of the aorta into the A. iliaca communis, and filled with approximately 1 mL of contrast agent. After filling the balloon, the T-valve was closed to maintain constant pressure. The catheter was then retracted to the distance between the two vertebral bodies (approximately 4 cm) with a velocity of approximately 1 cm/s. Prior to ballooning, heparin (500 U) was administered intravenously and repeatedly for 7 days after the procedure in the form of subcutaneous injections to prevent thrombosis. No additional antiplatelet therapy was administered in addition to heparin, and thrombosis was not observed.

On the same day, a high-cholesterol diet (HCD) was initiated and maintained for five weeks, during which the animals were fed an atherogenic diet consisting of 1% cholesterol. Of the 11 animals, one refused HCD and was excluded from further evaluation. After 5 weeks of HCD, the 10 remaining animals received normal chow for the remainder of the study (which varied for individual animals between 1 and 28 weeks; see Figure 1 and Table 1) to investigate the effect of plaque maturation and vulnerability on nanoparticle accumulation.

Following the surgical procedure, the region of vessel injury was monitored using the CT angiography system at week 3 and, where applicable, at week 11 after balloon injury. The lumen diameters on the 3D images were measured along the injured region in the sagittal and coronal planes to monitor lumen narrowing. Because the diameter of the aorta visualized with contrast agent-enhanced imaging is dependent on the image settings and age of the animals (older animals with a larger vessel diameter than younger animals), the image parameters of every image were set to enable a visually good contrast between the vessel signal (orange) and background (grayscale). Measurements of the lumen diameters were then performed every five millimeters starting from a visually unaltered area (which was distal to, but near, the A. renalis) towards the bifurcation of the aorta into the A. iliaca communis. The first measurement of A. renalis was set at 100%, and all other measurements were calculated relative to the reference measurement.

Table 1 Atherosclerotic Plaque Characteristics in the Experimental Rabbits

Animal No.	Plaque age (wk from balloon injury)	Normal diet Period Post HCD	Lumen Narrowing at Week 3 (%)	Plaque Area (mm^2)	Normalized Plaque Area (%)	Max Plaque Thickness (μm)	Intima: Media Thickness (IMT)	Minimum FC Thickness (μm)	Mean Macrophage load (%)	Maximum Macrophage Load (%)	Prussian Blue Score (Arbitrary Units)	CD31 Signal
1	6	1	16.3 (c) / 10.6 (s)	2.20	57.2	515	7.58	18.5	16.9	29.5	1	–
2	6.5	1.5	23.9 (c) / 27.6 (s)	0.35	12.5	146	0.57	24.8	4.7	6.9	1	–
3	12	7	12.6 (c) / 13.4 (s)	4.13	50.5	898	4.94	16.9	24.0	34.0	2	+ (i, m)
4	18	13	16.9 (c) / 12.9 (s)	3.73	42.5	583	3.97	12.6	26.4	36.1	2	+ (i, m)
5	18	13	17.7 (c) / 11.1 (s)	3.12	50.3	616	8.30	24.5	15.3	20.3	2	+ (i, m)
6	25	20	6.4 (c) / 10.5 (s)	2.96	39.4	634	4.81	10.4	20.0	28.5	4	+ (i)
7	27	22	30.5 (c) / 24.0 (s)	4.12	43.4	801	4.48	13.9	12.2	18.4	2	+ (m)
8	29	24	7.9 (c) / 7.9 (s)	1.74	36.3	563	7.93	11.9	25.1	30.6	4	(a)
9	33	28	27.7 (c) / 27.1 (s)	3.32	44.1	842	11.52	8.0	16.7	21.4	3	(a)
10	33	28	11.2 (c) / 11.0 (s)	1.71	50.9	368	4.23	8.0	22.6	29.2	3	+ (i, m)

Notes: Lumen narrowing: (c) maximal lumen decrease measured in the coronary plane; (s) maximal lumen decrease measured in the sagittal plane. Mean macrophage load: Average RAM-11-positive area as a percentage of total plaque area from all measured sections along the plaque. Maximum macrophage load: Maximum RAM-11-positive area as a percentage of the total plaque area in any plaque section. The Prussian blue score was evaluated using an arbitrary scale, with 0 indicating no signal, 1 indicating a weak signal, 2 medium signals, 3 strong signals, and 4 very strong signals. CD31 signal origin: (i) intima, (m) media, (a) adventitia.

Abbreviations: FC, fibrous cap; HCD, high-cholesterol diet; IMT, intima-media thickness.

https://doi.org/10.2147/IJN.S430693

Nanoparticle Administration and MRI

In eight of the 10 animals that completed HCD feeding, SPION^{dex} (2.6 mg iron/kg bw) was administered intravenously as a slow bolus (2 mL/min). As a reference SPION-based contrast agent, ferumoxytol (Feraheme®; 2.6 mg iron/kg bw) was administered intravenously to two randomly assigned animals (animals 9 and 10 in Table 1). The dose was chosen based on previous clinical studies of ferumoxtran. The total dose of iron injected in these studies corresponded to 195 mg iron for a 75-kg patient, which is less than the amount of iron in 1 U of transfused blood (200 mg). For comparison, the total body iron in humans is 3500 mg and the maximum total dose of intravenous iron dextran supplements is 20 mg iron/kg body weight,[20] which corresponds to 1500 mg iron for a 75-kg patient, and is thus 7.69-fold larger than the dose used for imaging.

MR of the rabbits was performed (a) directly before nanoparticle administration and (b) 24 h later using a 1.5 T scanner (Aera, Siemens Healthcare, Erlangen, Germany) with a 15-channel knee coil. The rabbits were anesthetized as described above (see 2.4), placed in the supine position (feet first), and immobilized using foam material. The protocol consisted of a 2D multi-slice T_1 fast low angle shot (FLASH) gradient echo sequence with fat suppression in transversal and coronal direction (0.625×0.625× 2.0 mm³, TE = 7.15 ms, TR = 342 ms, TA 7:06 min, FoV 130×160) and a susceptibility-weighted sequence (SWI) in transversal direction (0.58× 0.58×2.0 mm³, TE = 40 ms, TR = 49 ms, TA 5:18 min, FoV 150×150). All images were transferred to a dedicated postprocessing workstation for further image evaluation.

Histological and Immunohistochemical Staining

Following the MRI, anesthetized animals were euthanized with pentobarbital at a dose of 160 mg/kg body weight. Aortic specimens (total length of ca. 4–5 cm), containing the entire tunica intima, tunica media, and part of the adventitia, were cut into five equal segments of equal length, labelled 1–5, starting at the aortic bifurcation and placed in embedding cassettes. The aorta segments were fixed in 4% formaldehyde solution (Roth) in PBS for five days, dehydrated in an ascending isopropanol series, and embedded in paraffin. Sections of 5 µm thickness were cut using a microtome, placed on silane-coated slides, dewaxed in xylene, rehydrated in ethanol, and washed with Tris-buffered saline containing 0.1% Tween 20 (TBS-T). The sections were stained using a catalyzed signal amplification (CSA) system (Dako) with diaminobenzidine (DAB) as a chromogene. A mouse monoclonal antibody against rabbit macrophages (RAM-11, 1:50 dilution) was used to detect plaque macrophages and a mouse monoclonal anti-CD31 antibody (clone JC/70A) was used to detect vasa vasorum. Smooth muscle cells were detected using anti-smooth muscle actin antibody (clone 1A4). Tissue specimens were counterstained with hematoxylin and mounted on a durable medium (Aquatex, Merck).

Crossman's trichrome staining of muscle and collagen was used to characterize the tissue composition of the arterial specimens. Using this method, the cytoplasm and muscle tissue were stained red, the nuclei of all cells were stained black, and the collagen fibers were stained green. The arterial sections were immersed in hematoxylin for 10 min, followed by rinsing with tap water for 10 min. Subsequently, the samples were immersed for 1 min in a mixture of acid fuchsine and acridine orange solution and subsequently washed with distilled water. The resulting red stain was differentiated using 1% phosphomolybdic acid until the connective tissue was decolorized. Subsequently, the samples were stained with light-green light green was performed for 5 min. Following washing and dehydration in an isopropanol gradient and xylene, staining was performed using mounting medium (Roti-Histo Kit, Roth).

Plaque Morphometry and Image Analysis

Digital images of the specimens were obtained using an Axio Observer.Z1 microscope (Zeiss, Jena, Germany) and analyzed using the ImageJ software. To calculate the plaque area, the surface delimited by the internal elastic lamina was measured and the surface of the lumen was subtracted. In the analyzed sections, no plaque extension into the media was observed, and the internal and external elastic laminae remained intact and clearly visible. The results were normalized to the total vessel cross-sectional area for each arterial section to eliminate variations that could occur solely because of different vessel sizes. Minimum fibrous cap (FC) thickness and maximal media thickness were measured for each plaque section. Additionally, the intima-to-media thickness (IMT) was calculated.

To analyze the macrophage load in the plaques, MetaVue software was used (Molecular Devices LLC, San Jose, CA, USA). Using this software, the color threshold for DAB-immunostained cells in the images was manually adjusted until computerized detection matched visual interpretation. The analyses were performed by two independent observers (AS

and IC). The intra- and inter-observer variabilities were < 10%. Macrophage burden was normalized to the respective plaque area and expressed as a percentage of the macrophage load.

Evaluation of Iron Content by Histology

To assess the presence of SPIONs in tissues, paraffin sections of harvested organs (liver, spleen, heart, and kidney) and arterial sections were stained with Prussian blue dye. Paraffin-embedded serial sections of 5 µm thickness were cut, dewaxed in xylene, rehydrated in ethanol, and subsequently stained with a 1:1 solution of hydrochloric acid (2%) and potassium ferrocyanide (2%). After 30 min at RT, the nuclei of the cells and cytoplasm were counterstained with Fast Red and rinsed with distilled water. The samples were then dehydrated in an isopropanol gradient and xylene, and mounted (Roti-Histo Kit). Owing to the low contrast of the blue signal in histological staining, the iron load in the respective plaques was evaluated using an arbitrary scale. Briefly, the images were compared and the samples with the highest intensity were assigned as "4", indicating a very strong signal. Images with the weakest blue staining were classified as "1" or as weakly positive. The remaining images with intermediate staining were compared to each other and grouped as "2" (medium signal), or "3" (strong signal) on an arbitrary scale. The evaluation was performed independently by two researchers and was checked for consistency.

In vitro Safety

Cells

Human umbilical vein endothelial cells (HUVECs) were freshly isolated from umbilical cords collected post-partum (kindly provided by the Dept. of Gynaecology, University Hospital Erlangen) and cultured according to a standard technique.[40] The use of human material was approved by the local ethics committee of the Universität Erlangen-Nürnberg (review number 16–335_2-B from 22.11.2016). HUVECs at passage 1–2 were used for all in vitro experiments.

Real-Time Cell Analysis

The xCELLigence system (RTCA DP Analyzer, Roche Diagnostics, Mannheim, Germany) was used to monitor the effects of nanoparticles on HUVEC viability, essentially as described before in:[41]

> Experiments were performed in 16-well E-plates (ACEA Bioscience, San Diego, USA), in which the impedance is measured with the help of microelectrodes localized at the bottom of the wells. For background measurements, 100 µL cell-free endothelial cell growth medium was added to each well. Afterwards, 50 µL of medium from each well was replaced with 50 µL of a cell suspension containing $1x10^3$ HUVECs. Approximately 30 min after seeding the cells, impedance monitoring was initiated using the xCELLigence system. At 24 h after seeding, an additional 100 µL of media containing different concentrations of nanoparticles was added to the wells as follows: (a) for controls, 100 µL of pure medium without nanoparticles, and (b) for the treatment samples, 100 µL of medium containing nanoparticles at concentrations 2x higher than the required final nanoparticle concentration[41].

The final ferumoxytol concentration was0, 25, 50, 100, 200, and 400 µg Fe/mL. $SPION^{Dex}$ was used at the corresponding concentrations. Experiments were performed using hexaplicate samples. Cell growth was monitored using this setup by measuring the impedance every 10 min for 96 h.

Flow Experiments

Flow cytometry experiments were performed as previously described.[42] The effects of ferumoxytol and $SPION^{Dex}$ at two different concentrations (100 and 400 µg/mL) were compared. Subsequently, F-actin in HUVECs was visualized using Alexa488-phalloidin (PromoKine, Heidelberg, Germany) and cell nuclei were stained with DAPI (Molecular Probes, Darmstadt, Germany). Images were obtained using a Zeiss Axio Observer.Z1 (Carl Zeiss AG). To determine confluence, images taken at x10 objective magnification were analyzed using ImageJ software.

In vivo Toxicity Study in Rats

To determine the possible toxic effects of SPION^{Dex} formulation and to identify the nanoparticle doses corresponding to the No Observed Adverse Effect Level (NOAEL) and to the Maximum Tolerated Dose (MTD), a single-dose intravenous administration study was performed in rats.

All the procedures involving the animals were conducted according to national and international regulations (L.D. 26/2014; Directive 2010/63/EU) under authorisation no. 16/2015-PR, released on March 07, 2017, by the "Direzione Generale della Sanità Animale e dei Farmaci Veterinari, Ufficio VI" from the Italian Ministry of Health.

Animals

Twenty-eight Sprague-Dawley OFA (SD) rats (14 animals/sex; aged 5 weeks; weight between 102 g −151 g) were purchased from Charles River Italia, Calco (Lc, Italy). Animals were housed under controlled conditions at a temperature of 22 °C ± 2 °C, humidity of 55% ± 10%, and 12-h light/dark cycles. Food pellets and filtered water from municipal services were provided ad libitum. After 7 days of acclimation, animals were randomly assigned to one of four exposure groups (3 animals/group/sex): group 1 (10 mg Fe/kg), group 2 (30 mg Fe/kg), group 3 (60 mg Fe/kg) and group 4 (100 mg Fe/kg). All rats received a single intravenous injection of SPION^{Dex} at dose ranging from 1.5 to 15.1 mL/kg[43] via the tail vein at an injection rate of 2 mL/min using a Harvard infusion pump (Holliston, MA). Animals of each group were sacrificed after 2-week observation period.

Observation

On the day of dosing (Day 0), animals were individually inspected before and after dosing for any clinical signs or reactions to treatment. During the subsequent 2-weeks observation period, all animals were inspected once a day and weighed at Day 3, Day 7, Day 11 and at sacrifice.

Pathology

On the day of sacrifice, the animals were anesthetized with SevoFlo at an induction rate of 3 to 4% and subsequently by intramuscular injection of 0.20 mL/kg of Zoletil 50/50 (20 mg/kg) and 0.25 mL/kg of Rompun (5 mg/kg). Anesthetic doses were calculated based on the last recorded body weight. Animals were euthanized and bled after collection of blood from the abdominal aorta. After exsanguination, a complete macroscopic post-mortem examination was performed on all animals. Any abnormal findings were recorded.

Statistical Analysis

Data are expressed as mean ± SD unless stated otherwise. Before statistical analyses, the samples were tested for normality to avoid assumptions regarding data distribution and to select a suitable (parametric or non-parametric) test. Statistical significance was set at $P<0.05$. Spearman rank-order correlation test was used to analyze the correlations between different immunohistochemistry results and plaque age. Analyses were performed using the SigmaStat® software.

Results

Nanoparticle Properties

The nanoparticles produced had a polydispersity index (PDI) of 0.122 and a zeta-potential of −3,4 mV at neutral pH. In our previous studies, the size of SPION^{Dex} was tuned to ~ 30 nm by modifying the synthesis parameters.[31,32] The particles, with hydrodynamic size of 35 nm and PDI of 0.129, had transverse relaxivity values of 5.4 $mM^{-1}s^{-1}$ for r_1, 66 $mM^{-1}s^{-1}$ for r_2 and 101 for r_2* at 3T as reported before.[29] Transmission electron microscopy revealed that SPION^{Dex} particles had a non-spherical, chain-like morphology. The detailed characterization of these particles has been reported before[31,32] and is summarized in the SI (see Supplementary Figure 1 and Supplementary Table 1).

Ferumoxytol particles were characterized by a hydrodynamic size of 38.1 nm, PDI of 0.210, and highly negative surface charge (−40.1 mV). Ferumoxytol had transverse relaxivity values of 5.4 $mM^{-1}s^{-1}$ for r_1, 67 $mM^{-1}s^{-1}$ for r_2 and

98 for r_2* at 3T.[29] Both formulations were characterized by good colloidal stability in aqueous media, without signs of agglomeration or sedimentation.

Atherosclerotic Plaque Model

Following balloon injury, the progression of atherosclerosis in rabbits exposed to HCD was monitored using CT angiography as described in the Methods section (2.4). In the experimental animals included in this study, lumen irregularities and narrowing due to plaque formation were observed over time (Table 1). The duration of HCD (5 weeks) was kept constant for all experimental animals to accumulate a large amount of cholesterol in their organs. Afterwards, individual animals were placed on a normal diet for various periods of time (see also Figure 1) to reduce their cholesterol loading strain. This alternating diet approach was originally described by[44] and has been shown to result in atherosclerotic plaques with vulnerable features in other studies.[45,46] Notably, in our study, instead of selecting a fixed period of normal diet after the 5-week HCD, the duration of normal chow in the individual atherosclerotic animals varied between 1 and 28 weeks, which allowed observation of plaque progression and maturation depending on time. Table 1 summarizes the data of the individual animals, including age and size of the plaque, IMT, FC thickness, and macrophage burden. The results demonstrated that, although all animals received HCD for an identical period, there were considerable differences in plaque size and/or macrophage load. In particular, one of the two animals with the shortest normal diet periods (1–2 weeks post HCD) had a very small plaque with a low macrophage load. However, independent of plaque size, these animals had lesions rich in smooth muscle cells (Supplementary Figure 2) with a relatively thick fibrous cap and no neovascularization (Table 1). Importantly, despite a relatively short period of HCD compared with other studies,[44,45] extending the time of normal chow did not lead to spontaneous plaque regression; the lesions remained rich in macrophages, and progressive FC thinning took place. The correlations between plaque age and size, and between plaque size and macrophage burden are shown in Figure 2A–D. It was observed that the negative correlation of FC thickness was strongest with plaque age and moderate with mean macrophage load. The other parameters (intimal thickness and mean macrophage load) showed only weak positive correlations with the plaque age. We have subsequently divided the animals into two groups, those with younger plaques (6–18 weeks post ballooning), and those with older plaques (25–33 weeks) and compared their plaque morphology and macrophage load. As shown in Supplementary Figure 3, although there were no significant differences in plaque size, IMT or macrophage load between the two groups, the animals with older plaques had lesions with significantly thinner fibrous caps. Notably, as the plaque age progresses beyond 18 weeks, considerably less variation in plaque thickness, normalized area, or macrophage load is observed (Supplementary Figure 3).

SPION Accumulation in the Plaques

Prussian blue staining of arterial cross-sections confirmed the presence of USPIO in atherosclerotic lesions of all animals. Representative histological images of animals receiving USPIO^{Dex} or ferumoxytol are shown in Figure 3A and B, and quantification of the Prussian blue score is shown in Table 1. Of note, the intraplaque accumulation of SPIONs in animals with the youngest lesions was the weakest, whereas the strongest Prussian blue staining was observed in plaques that were 25 weeks and older (see also Supplementary Figure 3). Although ferumoxytol has been successfully used in human atherosclerosis imaging studies, one previous study[39] indicated that this formulation accumulates poorly in preclinical atherosclerosis in rabbits as compared with ferumoxtran-10. Our data did not confirm these findings, and ferumoxytol accumulation was detectable in two animals that received this formulation as a reference substance. Notably, the animals that received ferumoxytol had relatively old plaques (33 weeks), but their plaque vulnerability features did not differ from those animals administered SPION^{Dex} with plaque ages of/above 25 weeks. Correlation plots of iron content with plaque age and average macrophage burden detected in the histological sections along atherosclerotic plaques are shown in Figure 4A and B. A very strong positive correlation between the iron content and plaque age was detected, and a moderate positive correlation with the mean macrophage load was observed.

Iron Accumulation in Organs

Following sacrifice, the organs were harvested and analyzed for iron accumulation. Histologically, a strong accumulation of both SPION^{Dex} and ferumoxytol was detected in spleen and liver (Figure 5A), which are the main organs involved in

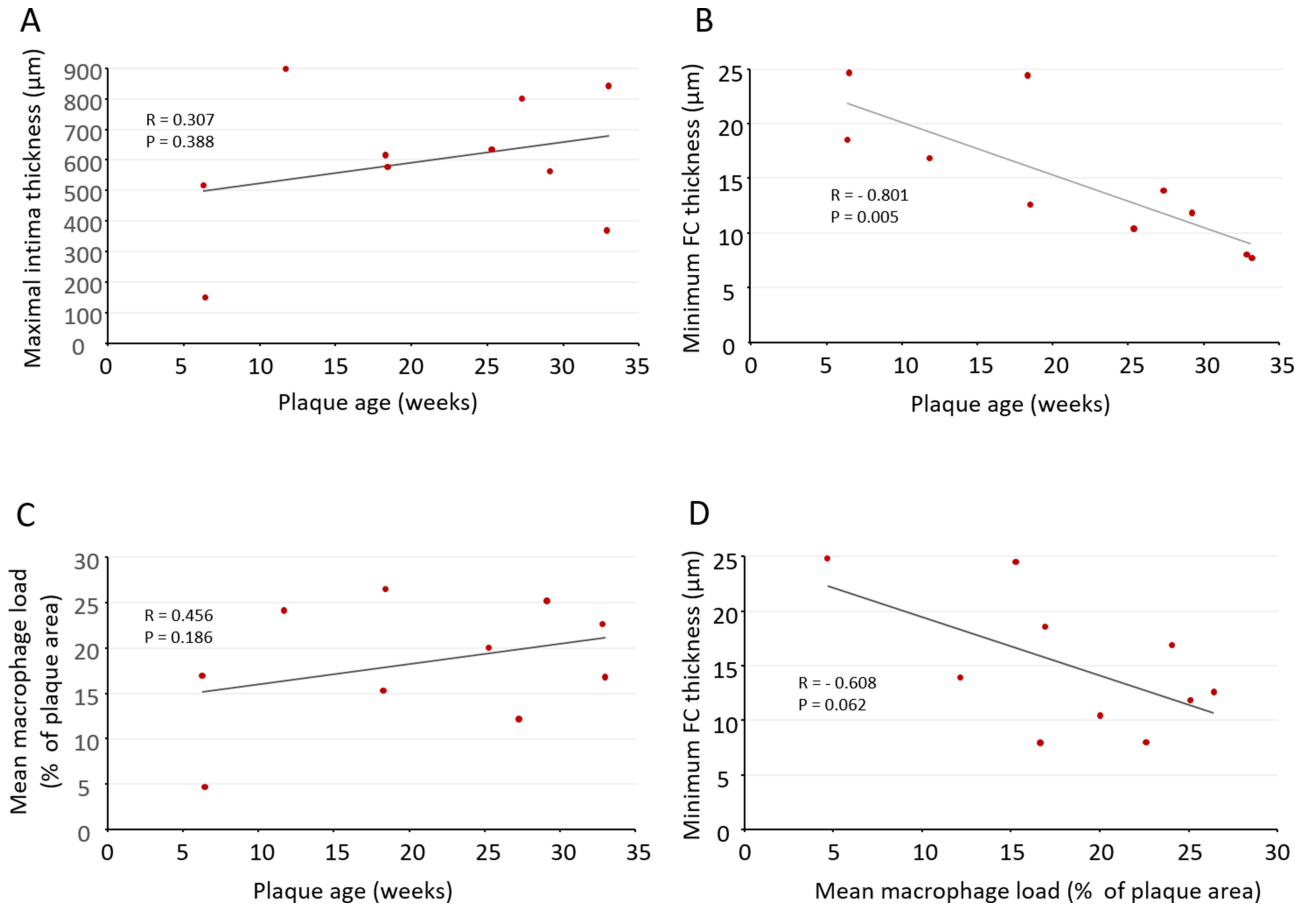

Figure 2 The correlations between plaque age and intima thickness (**A**), minimum FC thickness (**B**) and macrophage burden (**C**), as well as minimum FC thickness and macrophage load (**D**).

Notes: Rabbits were exposed to abdominal aorta ballooning, followed by HCD for 5 weeks. Afterwards, individual animals were fed normal chow for different amounts of time. Following SPION administration and MRI, animals were sacrificed and their atherosclerotic specimens were analyzed by histology/immunohistochemistry. The age of the plaque in weeks after ballooning for each animal is shown in Table 1. Spearman rank-order correlation test was used to analyze the correlations.

Abbreviation: FC, fibrous cap.

iron metabolism and clearance. In the majority of animals, a very weak positive iron signal was observed in the heart and kidney (Figure 5B), whereas in one animal, strong positive staining was detected in both kidneys (Supplementary Figure 4).

Detection of SPIONs Using MRI

SPION-related signal decrease was observed in all animals in the atherosclerosis-affected region of the abdominal aorta. The representative images are shown in (Figure 6A–D for $SPION^{Dex}$ and E-F for ferumoxytol-treated animals). Susceptibility triggered by $SPION^{Dex}$ was particularly evident in coronal images (Figure 6C). In comparison to the pre-application images (Figure 6F) a signal decrease in the distal abdominal aorta was observed after the administration of ferumoxytol (Figure 6H). The observed signal decrease in animals administered ferumoxytol was more pronounced than that in those treated with $SPION^{Dex}$ (Figure 6B), but a strong accumulation of ferumoxytol in the vertebral body was also observed (Figure 6H). This effect was observed in animals that received ferumoxytol but not in animals that received $SPION^{Dex}$.

In the SWI sequence (Figure 7A–D), both the abdominal aorta and inferior vena cava of $USPIO^{Dex}$-treated animals showed a strongly reduced signal (Figure 7B), which indicated that $SPION^{Dex}$ particles were still present in the circulating blood. Similar to the T_1 FLASH technique, 24 h after the administration of ferumoxytol, a reduced signal

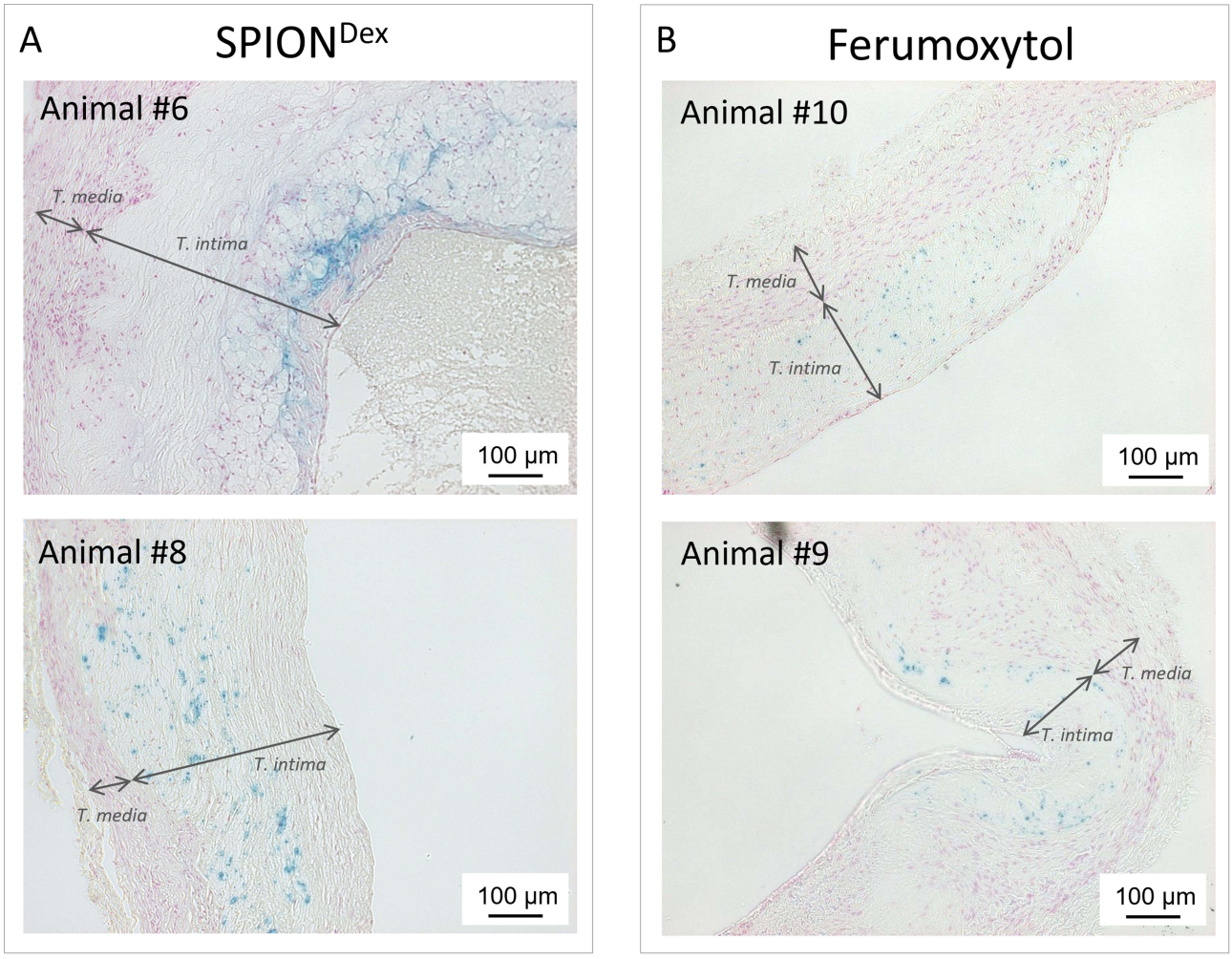

Figure 3 Tissue iron detected by Prussian blue staining in the atherosclerotic plaques at 26 h post-administration. The example histological images of animals receiving (**A**) $SPION^{Dex}$ or (**B**) ferumoxytol are shown.

Notes: Rabbits were exposed to abdominal aorta ballooning, followed by HCD for 5 weeks. Afterwards, individual animals were fed normal chow for different amounts of time. Following SPION administration and MRI, animals were sacrificed and the accumulation of SPIONs in atherosclerotic plaques was determined by Prussian blue staining. Tunica intima and tunica media in the atherosclerotic specimens are indicated with arrows. The age of the plaque in weeks after ballooning for each animal is shown in Table 1.

Abbreviations: HCD, high-cholesterol diet; MRI, magnetic resonance imaging; SPION, superparamagnetic iron oxide nanoparticles.

was observed in the vertebral bodies (See Figure 7D), but in contrast to T_1-weighted images, the signal decrease was no longer detectable in the vessels.

Nanoparticle Safety

In contrast to $SPION^{Dex}$, which was well tolerated upon injection, a bolus speed of 2 mL/min was clearly too fast for ferumoxytol administration. In the first of two ferumoxytol-receiving rabbits, a strong adverse reaction to the nanoparticle injection was observed. Stiffening of the extremities and the whole body occurred, and breathing was erratic and irregular. The patient's heartbeat was irregular and jerky. Signs of hypersensitivity reaction lasted for approximately 5 min, after which the condition of the animal started to normalize. Subsequently, a slower administration of ferumoxytol was performed in the second rabbit. No immediate adverse effects were observed with this protocol. However, very long muscle twitches were observed throughout the body during euthanasia (approximately 26 h post administration). The left foreleg continued to twitch for approximately 20–30 min after the death of the animal, even after most of the organs had already been removed.

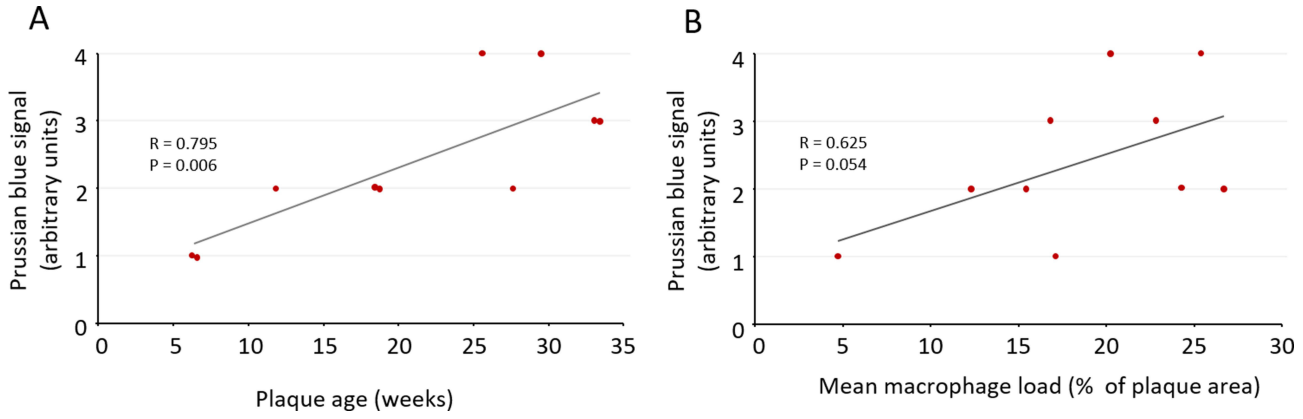

Figure 4 Correlations of iron content with plaque age (**A**) and mean macrophage burden (**B**).
Notes: Rabbits were exposed to abdominal aorta ballooning, followed by HCD for 5 weeks. Afterwards, individual animals were fed normal chow for different amounts of time. Following SPION administration and MRI, animals were sacrificed and their atherosclerotic plaques were stained with Prussian blue to detect SPIONs or with RAM-11 to detect macrophages. The age of the plaque in weeks after ballooning for each animal is shown in Table 1. Spearman rank-order correlation test was used to analyze the correlations.
Abbreviations: HCD, high-cholesterol diet; MRI, magnetic resonance imaging; SPION, superparamagnetic iron oxide nanoparticles.

In vitro Safety

To investigate whether hypersensitivity to ferumoxytol is associated with its cytotoxic effects on the endothelium, an in vitro study with primary human cells was performed. The biocompatibility of SPION^{Dex} has been extensively evaluated in our previous studies[31,47] and allowed their use as a nanosafety standard in comparison with ferumoxytol. In the first set of experiments (Figure 8A), real-time cell analysis after treatment with nanoparticles was performed. The cell index determined using impedance measurements reflects cell adhesion strength, viability, number, and morphology, and its steady increase was observed over time in control (untreated) endothelial cells. The growth curves of the cells treated with either ferumoxytol or SPION^{Dex} were similar to those of untreated control samples, showing a comparable increase in the cell index during the entire measurement period (72 h). Consequently, neither ferumoxytol nor SPION^{Dex} at concentrations of up to 400 µg/mL had any negative effects on endothelial cell viability, growth, or adherence. Live cell microscopy confirmed that ferumoxytol and SPION^{Dex} were well tolerated by endothelial cells. No negative effects of these particles on the morphology or confluence of cells were observed in comparison with untreated controls (Figure 8B).

To evaluate the effect of circulating particles on monolayer integrity, the endothelial monolayer was perfused with a medium containing 100 or 400 µg/mL ferumoxytol or SPION^{Dex} for 18 h. The effects of nanoparticles were compared in cells exposed to different types of shear stress (laminar shear stress in the straight part of the channel versus non-uniform shear stress at the outer walls of the bifurcations). Both ferumoxytol and SPION^{Dex} were well tolerated by endothelial cells at concentrations up to 400 µg/mL. The treatment did not significantly affect cell morphology or induce cell shrinkage or detachment during exposure to shear stress (Figure 8C). Only minor effects were detectable, indicating good tolerability of both formulations in vitro.

In vivo Toxicity

No adverse signs or symptoms were observed for animals of group 1 and 2 (treated with SPION^{Dex} 10 and 30 mg Fe/kg). At 60 mg Fe/kg, 5 of 6 animals (all females and two males) showed oedema of paws 5 min after SPION^{Dex} administration. Moreover, male animals with oedema also showed hypoactivity. After 30 min observation time, all animals showed oedema of paws, but recovery was achieved within 2–4 h from administration (Table 2).

At 100 mg Fe/kg all animals showed oedema of paws and muzzle and a few cases of hypoactivity, or palpebral closure and dyspnea between 5 and 30 min after dosing. The observed effects were transient and the recovery was achieved between 2 h to 1 day after SPION^{Dex} administration (Table 2).

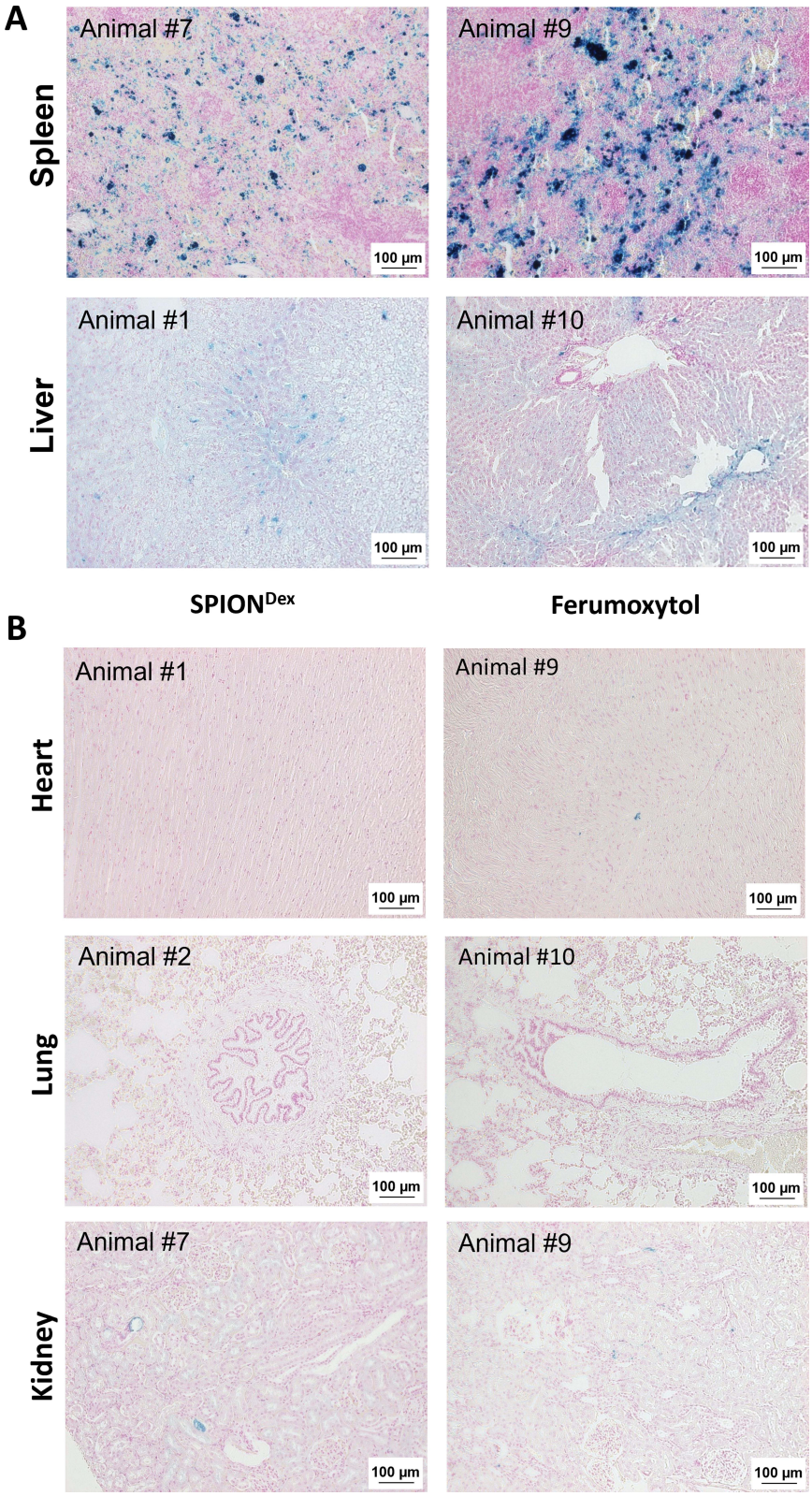

Figure 5 Accumulation of SPIONs at 26 h post-administration detected in the organs using Prussian blue staining. (**A**) Spleen and liver are the main accumulation sites of SPIONs; (**B**) none or only very weak iron signal is detectable by histology in heart, lungs or kidneys of SPION-treated rabbits. Images in the left panel show $SPION^{Dex}$-treated animals, images in the right panel images, ferumoxytol-treated animals.

Notes: Rabbits were exposed to abdominal aorta ballooning, followed by HCD for 5 weeks. Afterwards, individual animals were fed normal chow for different amounts of time. Following SPION administration and MRI, animals were sacrificed and the organs were collected to determine accumulation of SPIONs using Prussian blue staining. The age of the plaque in weeks after ballooning for each animal is shown in Table 1.

Abbreviations: HCD, high-cholesterol diet; MRI, magnetic resonance imaging; SPION, superparamagnetic iron oxide nanoparticles.

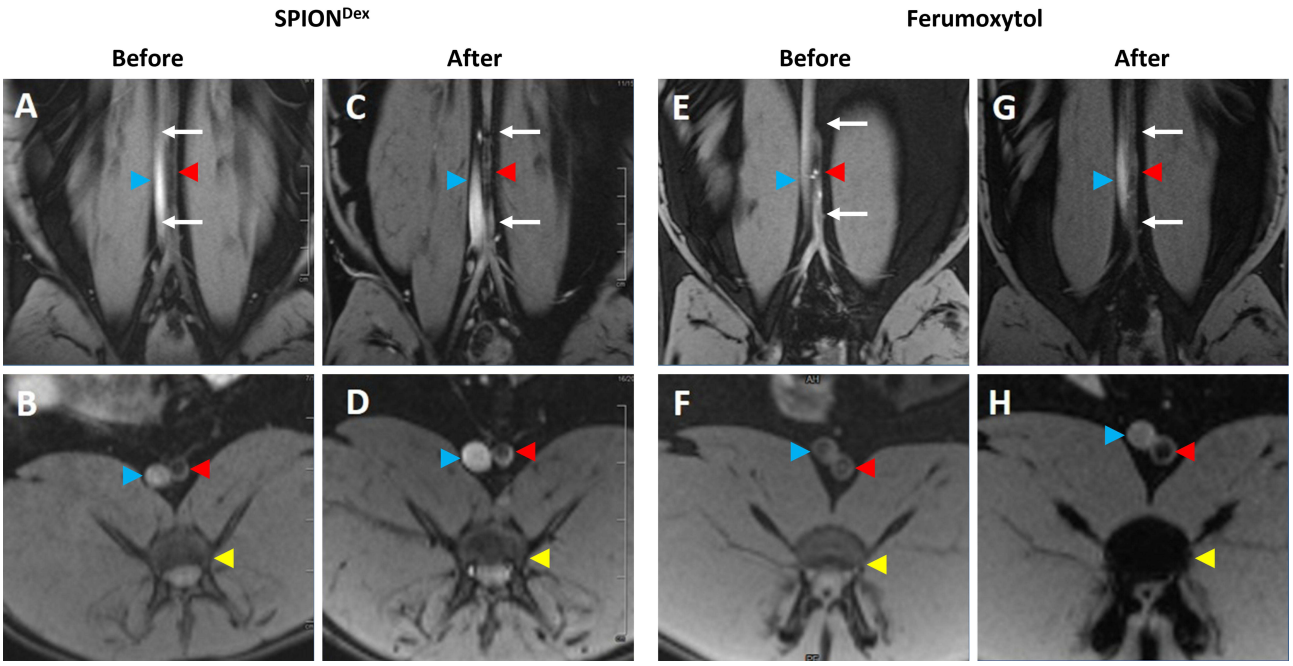

Figure 6 Coronal (**A**, **C**, **E** and **G**) and transversal (**B**, **D**, **F** and **H**) T_1-weighted images of distal abdominal aorta in two different atherosclerotic animals. (**A** and **B**) before $SPION^{Dex}$ administration and (**C** and **D**) 24 h after $SPION^{Dex}$ application; (**E** and **F**) before ferumoxytol administration and (**G** and **H**) 24 h after ferumoxytol application.
Notes: Rabbits were exposed to abdominal aorta ballooning, followed by HCD for 5 weeks. Afterwards, individual animals were fed normal chow for different amounts of time, followed by SPION administration and MRI, according to the scheme indicated in Figure 1. White arrows indicate the plaque region of abdominal aorta; red arrowheads: abdominal aorta; blue arrowheads: inferior vena cava; yellow arrowheads: vertebral bodies.
Abbreviations: HCD, high-cholesterol diet; MRI, magnetic resonance imaging; SPION, superparamagnetic iron oxide nanoparticles.

No changes in body weight (Figure 9A and B) or body weight gain were observed during the study among different treatment groups. All animals treated with $SPION^{Dex}$ doses higher than 10 mg Fe/kg showed mild (30 mg Fe/kg) to marked (60 and 100 mg Fe/kg) increase in lymph node volume and dark brown coloration of medial iliac, lumbar aortic, caudal and mesenteric lymph nodes (Table 2). Based on these results the NOAEL for a single intravenous administration of $SPION^{Dex}$ formulation in rats was considered to be 10 mg Fe/kg and the MTD higher than 100 mg Fe/kg.

Discussion

In this study, we performed a detailed characterization of a rabbit model of atherosclerosis to provide a more reproducible tool for the analysis of nanoparticulate contrast agents for atherosclerotic plaque imaging. Our previous studies showed that during 5 weeks of HCD following balloon injury, a very large amount of cholesterol is deposited in many organs and may persist for several weeks. Cholesterol loading during HCD generates a large health burden for rabbits, and the capability of individual animals to handle this burden is diverse. To reduce the hyperlipidemic strain and systemic toxicity in the animals, we introduced a 2-week period of normal chow after HCD.[48] Alternating HCD (8 weeks) and a normal diet (6 months), while reducing systemic lipid toxicity, was previously shown to increase aortic atheroma in rabbits[44] and to enable triggering of plaque rupture. The model reported in 1960 was subsequently modified by other investigators to combine balloon injury with 2 months of HCD followed by 2 months[45] or 4 weeks of normal chow.[46] However, previous studies commonly applied a fixed duration of normal chow and did not investigate the relationship between an extended period of a normal diet and plaque progression or contrast agent accumulation. Our histological and immunohistochemical analyses demonstrated that animals fed a short-term normal diet period (1–2 weeks post HCD) had atherosclerotic plaques with relatively early features, including large variability in size, thicker fibrous cap, and no neovascularization. In line with this, SPION accumulation detected by histology was the lowest in these lesions, which may indicate that plaque permeability may still be insufficient for their entry at this stage. Similar findings were previously observed in a study investigating ferumoxytol-enhanced imaging, where only a very weak accumulation of this agent in atherosclerotic plaques after 2, 4, or 8 weeks of HCD was detected, despite the high administered dose

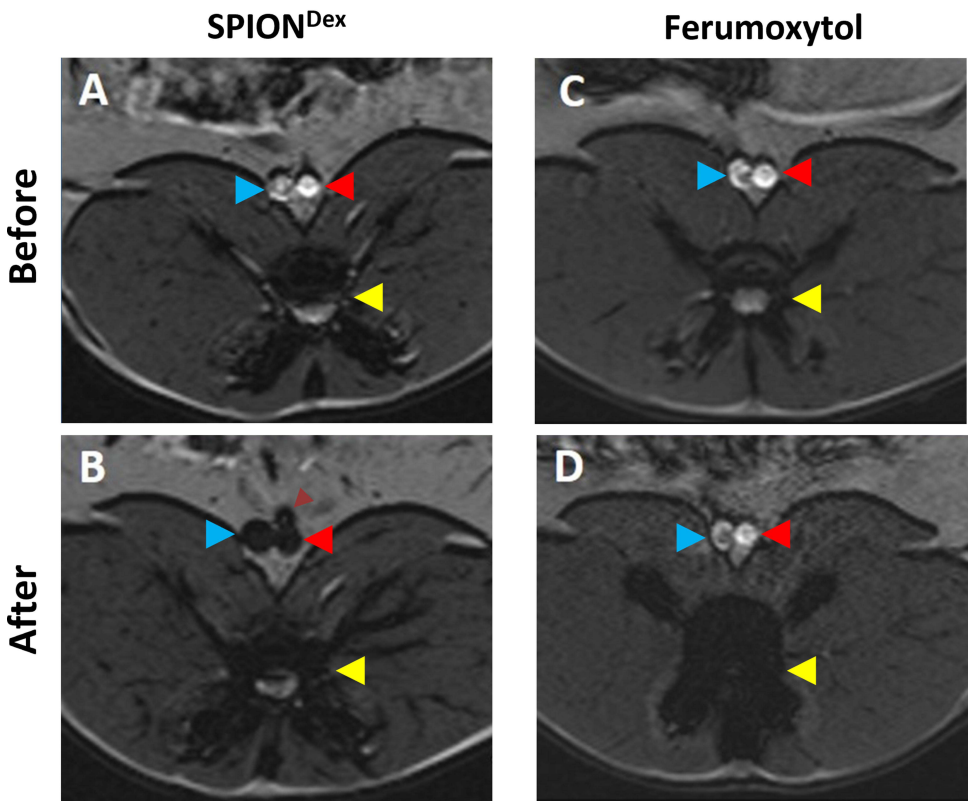

Figure 7 Axial slices of the distal abdominal aorta in SWI technique in two atherosclerotic animals. (**A**) before SPION^{Dex} administration and (**B**) 24 h after SPION^{Dex} administration; (**C**) before ferumoxytol administration and (**D**) 24 h after ferumoxytol administration.
Notes: Rabbits were exposed to abdominal aorta ballooning, followed by HCD for 5 weeks. Afterwards, individual animals were fed normal chow for different amounts of time, followed by SPION administration and MRI. Red arrowheads indicate abdominal aorta; blue arrowheads: inferior vena cava; yellow arrowheads: vertebral bodies. A smaller branching artery indicated with a small dark red arrowhead is visible in the panel B (possibly left colic artery or inferior mesenteric artery).
Abbreviations: HCD, high-cholesterol diet; MRI, magnetic resonance imaging; SPIO, superparamagnetic iron oxide nanoparticles.

(28 mg/kg).[39] Importantly, extending the normal diet time following cholesterol overloading did not lead to spontaneous plaque regression, even in animals fed normal chow for over 20 weeks after HCD. Plaque morphometry demonstrated that plaque size did not change with time, and intimal thickness was only weakly correlated with plaque age, confirming that atherosclerotic plaque growth is not a linear process. There was also a slight increase in the mean macrophage load in the older plaques. However, progressive FC thinning, reflected by a strong negative correlation between the FC thickness and plaque age, occurred over time. Another feature of advanced atherosclerosis is that neovascularization is more often detected in older plaques. In line with this, the highest SPION accumulation was observed in plaques that were 25 weeks old and older. In the previous studies, the uptake of dextran-coated ferumoxides[49] and other polyethylene glycol-coated formulations[37] via macrophage scavenger receptor (SR)- A1 was reported. As both SPION types used in our study contain dextran in their shell, we expected a strong correlation of the Prussian blue signal with the macrophage burden. However, the correlation of plaque iron content was stronger with plaque age than with the mean macrophage load. This was likely related to the fact that both FC thinning and neovascularization, which are also features of plaque vulnerability in humans, contribute to increased permeability to nanoparticulate contrast agents. This facilitates the enhanced entry of particles into the lesions, whereby some, but not all, are internalized by plaque macrophages. Additionally, SPIONs can be also be internalized by circulating monocytes, followed by their homing to the plaques. The different entry routes and entry time, as well as the differences in particle internalization by plaque-residing foam cells result in the differences in Prussian blue signal distribution, as shown in Figure 3, where apart from more punctuated, cell-bound staining, also regions of diffuse tissue staining are visible.

Previous clinical trials using ferumoxtran for MRI of carotid plaques have confirmed that SPION-based contrast agents can effectively detect and characterize atherosclerotic plaques, relying mainly on SPION uptake by activated

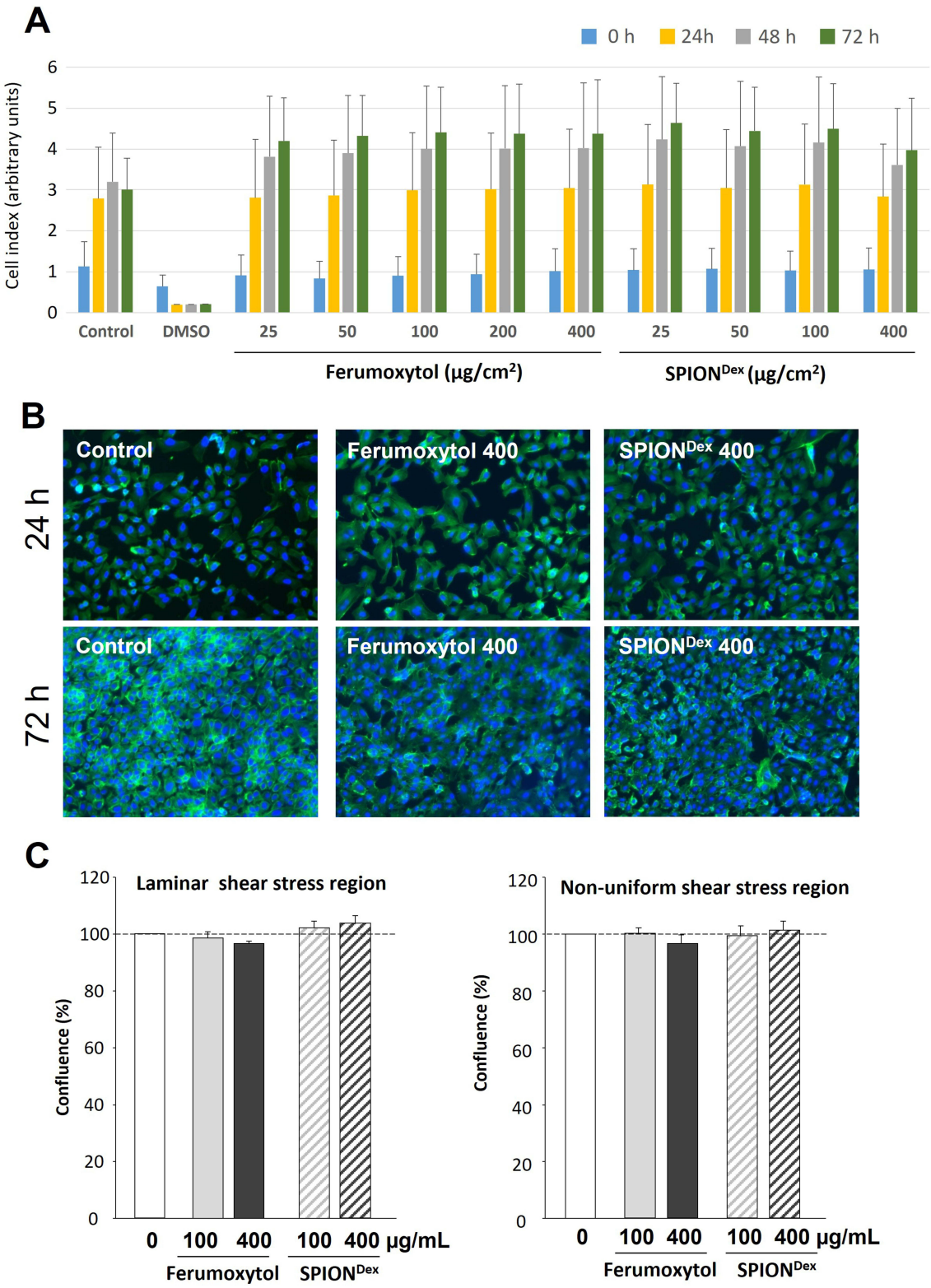

Figure 8 In vitro effects of SPION^{Dex} and ferumoxytol on primary HUVECs. (**A**) Real-time monitoring of cell index; (**B**) Corresponding live-cell imaging at high concentrations of nanoparticles (400 µg/cm^2); (**C**) Cell confluence under arterial like shear stress conditions. Control, medium only.

Notes: For (**A**), the mean ± SD of n=3 independent experiments with hexaplicate samples is shown. For (**C**), mean ± SD of n=3 independent experiments with duplicate samples is shown.

Abbreviation: SPION, superparamagnetic iron oxide nanoparticles.

Table 2 Single Dose Toxicity Study of SPION^{Dex} After Intravenous Administration in Rats

	Time	10 mg Fe/kg	30 mg Fe/kg	60 mg Fe/kg	100 mg Fe/kg
Body weight gain in g (male/female)	0–14 d	114.3 ± 3.2 /34.0 ± 5.6	121.3 ± 4.9 /33.3 ± 9.7	107 ± 13 /30.7 ± 3.8	108 ± 12 /27.0 ± 7.5
Clinical signs: Hypoactivity (male/female)	5 min	0 / 0	0 / 0	2 /0	1 /2
	30 min	0 / 0	0 / 0	0 / 0	0 / 0
	1–2 h	0 / 0	0 / 0	0 / 0	0 / 0
	1–14 d	0 / 0	0 / 0	0 / 0	0 / 0
Clinical signs: Dyspnoea (male/female)	5 min	0 / 0	0 / 0	1 / 0	1 / 0
	30 min	0 / 0	0 / 0	0 / 0	1 / 0
	1–2 h	0 / 0	0 / 0	0 / 0	0 / 0
	1–14 d	0 / 0	0 / 0	0 / 0	0 / 0
Clinical signs: Paw oedema (male/female)	5 min	0 / 0	0 / 0	1 / 3	3 /3*
	30 min	0 / 0	0 / 0	3 / 3	3 / 3*
	1–2 h	0 / 0	0 / 0	3 / 3	3 / 1*
	1–14 d	0 / 0	0 / 0	0 / 0	0 / 0*
Gross pathology: Lymph node discoloration (male/female)	14 d	0 / 0	3 / 3 #dark brown	3 / 3 ##dark brown	3 / 3 ##dark brown
Gross pathology: Lymph node volume (male/female)	14 d	0 / 0	3 / 3 #mild increase	3 / 3 ##marked increase	3 / 3 ##marked increase

Notes: Rats were intravenously administered a single dose of SPION^{Dex} (10, 30, 60 or 100 mg Fe/kg body weight, n=6 animals per group). Afterwards, the clinical signs and body weight of the animals were monitored for 14 days, followed by sacrifice and gross pathology examination. *Paw and muzzle oedema at 100 mg Fe/kg. #30 mg Fe/kg: Discoloration of medial iliac lymph nodes, lumbar aortic lymph nodes and caudal lymph nodes. ##60 and 100 mg Fe/kg: Discoloration of medial iliac lymph nodes, lumbar aortic lymph nodes, caudal lymph nodes and mesenteric lymph nodes.

Abbreviation: SPION, superparamagnetic iron oxide nanoparticles.

macrophages.[14,15,17] Importantly, SPION-enhanced MRI was also shown to be capable of detecting inflammatory activity in asymptomatic patients[50,51] and to identify inflammation within otherwise morphologically "stable" carotid plaques.[16] More recently, ferumoxytol-enhanced MRI has been shown to enable characterization of atherosclerotic plaque inflammation.[3,26] However, iron-oxide-based contrast agents have not been widely used in the field of cardiovascular imaging. For clinical applications, intravenous contrast agents must have appropriate imaging and pharmacokinetic properties, in addition to being characterized by low toxicity and very good hemocompatibility. Concerning the relaxivity, r_2 values varying between 60.8 $mM^{-1}s^{-1}$[52] and 89 $mM^{-1}s^{-1}$[53] at 1.5T were previously reported for ferumoxytol, and r_2* value of 60.4 $mM^{-1}s^{-1}$.[52] In a direct comparison at 3T, ferumoxytol (67 $mM^{-1}s^{-1}$ for r_2 and 98 for r_2*) and SPION^{Dex} (66 $mM^{-1}s^{-1}$ for r_2 and 101 for r_2*) had comparable relaxivity values, which indicates that at similar concentrations of SPION^{Dex} as of eg ferumoxytol, comparable signal alteration should be observed.[29] Despite this, certain differences in SPION-related MRI signal decrease between different formulations can be expected in vivo because of the diverse kinetics and blood circulation time,[39] which in turn affects tissue accumulation and, thus, the final MRI signal in tissue. Administration of ferumoxytol to rabbits led to a more pronounced signal reduction in the atherosclerotic abdominal aorta than SPION^{Dex}. This effect was also observed in our previous study in rat liver, where administration of SPION^{Dex} reduced the MRI signal but did not completely eliminate the visibility of anatomical structures.[29] Notably, a persistent reduction in MRI signal in vertebral bodies, but not in large vessels, was observed 24 h post ferumoxytol administration, which was the opposite in the rabbits treated with SPION^{Dex}. These results

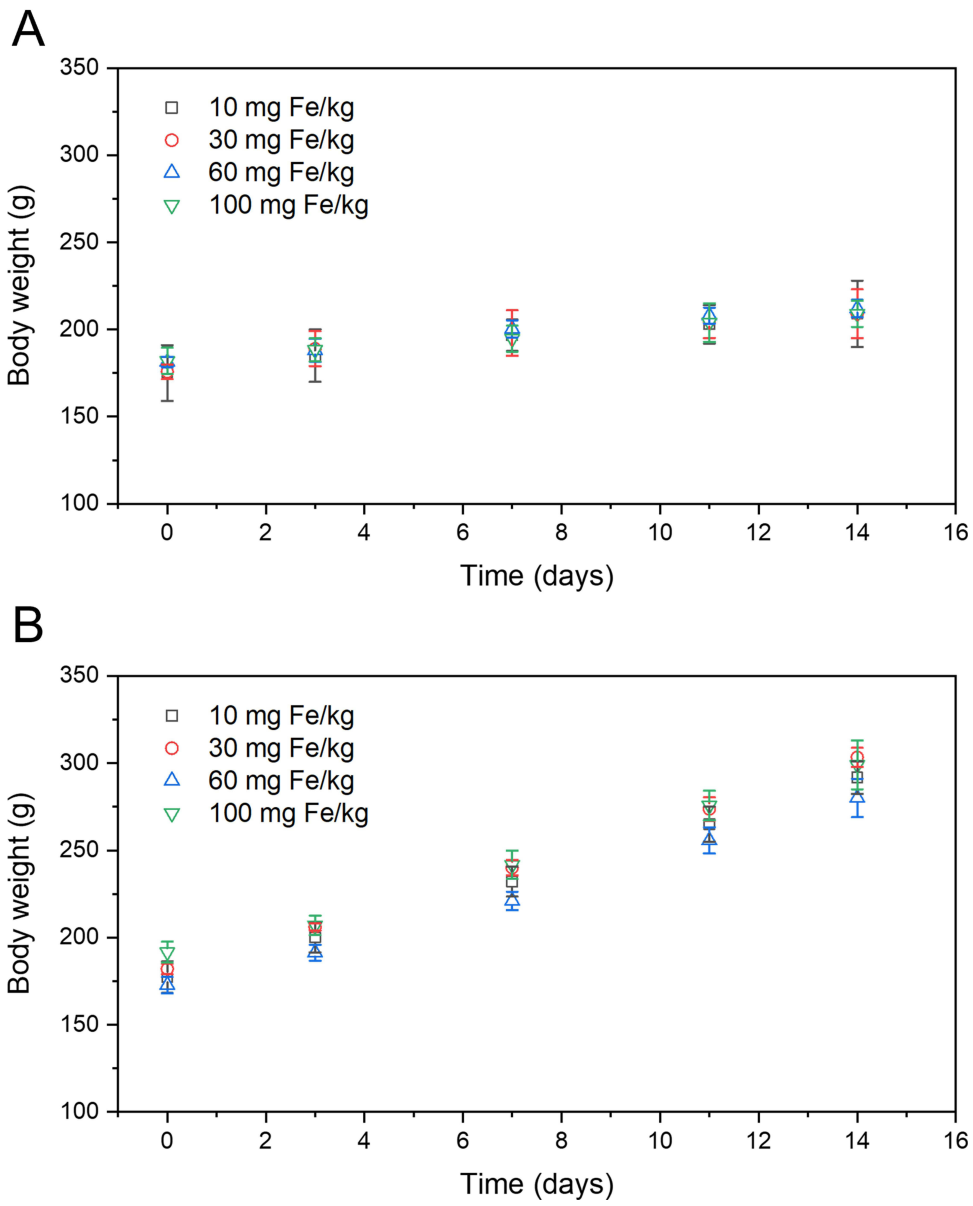

Figure 9 Effects of SPION^{Dex} administration on the body weight in healthy rats. (**A**) Female animals; (**B**) Male animals.
Notes: Rats were intravenously administered a single dose of SPION^{Dex} (10, 30, 60 or 100 mg Fe/kg body weight, n=6 animals per group). Afterwards, the clinical signs and body weight of the animals were monitored for 14 days.
Abbreviation: SPION, superparamagnetic iron oxide nanoparticles.

indicate that SPION^{Dex} may have a longer circulation time, while ferumoxytol is cleared faster from the blood, causing a persistent signal decrease in tissues.

However, it must be noted that a quantitative evaluation of MRI signals was not possible in this study due to technical limitations, including low resolution. Optimizing the MRI sequences and increasing the image resolution will be necessary in the future to enable the correlation of the MRI signal decrease with plaque age and macrophage load. Alternatively, quantitative MRI approaches, such as $T_2^{(*)}$ mapping, preferably using 3D isotropic sequences, may further improve the assessment of SPION accumulation from pre- and post-contrast scans.[26,27] However, the feasibility of such methods in preclinical models of abdominal aorta atherosclerosis has not been evaluated. A further technical problem was the slight signal reduction in the aorta region in the center of the images acquired before the administration of the particles. Because of anatomical reasons and the shape of the spine, this region of the aorta was slightly bent to the front

and, therefore, somewhat out of the coronal plane in which the images were taken, resulting in an apparent, non-specific reduction of the signal in this area. Although this signal artifact differs from the patchy signal decrease observed due to the presence of SPION infiltrating the plaque 24 h post-administration, in the future studies imaging in the sagittal plane may be necessary to avoid such artifacts.

In a clinical scenario, the extended circulation time of SPION-based contrast agents results in a relatively long time between particle administration and MRI scanning, which may not always be practical in terms of patient management. However, such long circulating ultrasmall particles have a better chance of penetrating the lesions, thus providing important information regarding plaque permeability, which is in turn related to instability.[3,54] In addition, it must be noted that while balloon injury and plaque development in the rabbit model were initiated at an aortic position below the liver, the accumulation of iron oxide in the liver of patients may potentially create issues during imaging atherosclerosis in the abdominal aorta, as signal voids from the liver may mask the region of interest. Therefore, relevant anatomical differences between species must be reckoned before clinical translation. Apart from this, it important to acknowledge that rabbit or porcine models of atherosclerosis do not reproduce human lesions very exactly, as the balloon injury, the short duration of plaque development and a low number of risk factors, all lead to very lipid-rich plaques, without major calcifications or inflammatory plaque shoulders typical for human plaques.[55] Nonetheless, those models effectively reproduce the typical vulnerability features such as FC thinning and neovascularization, especially in advanced plagues.

The potential to induce hypersensitivity reactions or complement activation involving lectin or the classical pathway,[56–58] is one of the major safety issues associated with iron oxide-based contrast agents.[56,58] Despite the overall good safety profile of the previously approved SPION formulations, injectable nanoparticles may cause moderate to strong anaphylactic reactions upon administration. Our observations of hypersensitivity reactions upon ferumoxytol injection in rabbits are consistent with the reported hypersensitivity to ferumoxytol in humans, which brought about several cases of lethal anaphylactic reactions and resulted in the strongest warning issued by the FDA in 2015.[59] As demonstrated in our recent study, ferumoxytol is a strong inducer of complement activation in human blood in vitro and complements activation-related pseudoallergy (CARPA) in healthy pigs.[29] In contrast, no activation of the complement system, either in vitro or in vivo was observed in the presence of SPION^{Dex}. The results of our present in vivo toxicity study in rats further underscore the outstanding safety of this formulation. While the starting dose of SPION^{Dex} (10 mg Fe/kg, which was nearly 4 times higher than SPION dose commonly used for clinical imaging) corresponded to NOAEL in rats, the highest tested dose (100 mg Fe/kg) was still lower than the MTD. It must be noted that 100 mg Fe/kg corresponded to 40 times the human expected clinical dose on body weight (BW) basis, and to about 6 times the human expected clinical dose (125 mg Fe/patient, corresponding to 2.5 mg Fe/kg for a 50 kg-subject) on the basis of Body Surface Area (BSA), according to the extrapolation factor set for rats in FDA Human Equivalent Dose (HED) guidance.[60] Collectively, our findings indicate that SPION^{Dex} formulation has a very good safety profile and is well tolerated upon administration in vivo, without inducing either mortality or persisting adverse clinical signs even at 100 mg Fe/kg.

Conclusion

The findings of this study indicate that extending the post-ballooning, post HCD period of the normal diet leads to the development of more advanced plaques with vulnerable features, even without extending the fixed 5 week-period of HCD. In rabbits, older and macrophage-rich atherosclerotic plaques with thin fibrous caps constitute a particularly useful model for investigating iron oxide-based contrast agents for MRI. Differences in tissue accumulation and MRI signals between different contrast agents were detectable in this model. Our data further indicate that, with optimized image quantification protocols, SPION-enhanced imaging can be used as a readout of plaque inflammation, as their increased uptake is associated with vulnerable features, such as macrophage accumulation, permeability, and neovascularization. Despite some differences in kinetics, both the new agent, SPION^{Dex} and the reference particle, ferumoxytol, showed good accumulation in atherosclerotic plaques after 24 h. However, in contrast to SPION^{Dex}, ferumoxytol can remain in tissues for long periods of time, which could complicate signal quantification in case of repeated administration. Moreover, the intravenous administration of SPION^{Dex} was better tolerated by experimental animals. Therefore, these particles will be further developed for clinical translation as a safe and non-immunogenic formulation, which offers the possibility of repeated administration and disease monitoring.

Data Sharing Statement

The raw data supporting the conclusions of this study are made available upon request to IC.

Ethics Statement

The rabbit study protocol was approved by the responsible authority (Regierung von Unterfranken, Würzburg, permission RUF-55.2.2-2532-2-549-12). The rabbit study was conducted under authorisation no. 16/2015-PR, released on March 07, 2017, by the "Direzione Generale della Sanità Animale e dei Farmaci Veterinari, Ufficio VI" from the Italian Ministry of Health.

The use of human material was approved by the local ethics committee (Ethikkommission der Friedrich-Alexander-Universität Erlangen-Nürnberg, review number 16-335_2-B from 22.11.2016). Informed consent was obtained from all the donors.

Acknowledgments

This work was supported by the 7th European Framework Program within NanoAthero project (Christoph Alexiou, Iwona Cicha, Erik Stroes, grant number: FP7-NMP-2012-LARGE-6-309820), the Deutsche Forschungsgemeinschaft (DFG, *German Research Foundation*) projects CI 162/2-3 and AL552/8-1, the Manfred Roth Stiftung, Fürth, Germany and the "Forschungsstiftung Medizin am Universitätsklinikum Erlangen", Erlangen, Germany.

The authors thank Dr. Marina Pöttler, Bianca Weigel, and Julia Band for help with animal experiments and Eveline Schreiber for help with the nanoparticle preparation. The present work was performed in partial fulfillment of the requirements for obtaining the degree "Dr. med". by A. S. and S. B. at Friedrich-Alexander University Erlangen-Nürnberg (FAU), Germany.

Author Contributions

All authors made a significant contribution to the work reported, whether that is in the conception, study design, execution, acquisition of data, analysis and interpretation, or in all these areas; took part in drafting, revising or critically reviewing the article; gave final approval of the version to be published; have agreed on the journal to which the article has been submitted; and agree to be accountable for all aspects of the work.

Disclosure

The authors report no conflicts of interest in this work.

References

1. Global Burden of Disease Study C. Global, regional, and national incidence, prevalence, and years lived with disability for 301 acute and chronic diseases and injuries in 188 countries, 1990–2013: a systematic analysis for the Global Burden of Disease Study 2013. *Lancet*. 2015;386:743–800. doi:10.1016/S0140-6736(15)60692-4
2. Jackson SA, Thomas RM, Harrison SN. *Cross-Sectional Imaging Made Easy*. 2nd ed. Churchill Livingstone; 2004.
3. Zheng KH, Schoormans J, Stiekema LCA, et al. Plaque permeability assessed with DCE-MRI associates with uspio uptake in patients with peripheral artery disease. *Jacc Cardiovasc Imag*. 2019;12:2081–2083. doi:10.1016/j.jcmg.2019.04.014
4. Rogosnitzky M, Branch S. Gadolinium-based contrast agent toxicity: a review of known and proposed mechanisms. *Biometals*. 2016;29:365–376. doi:10.1007/s10534-016-9931-7
5. Khawaja AZ, Cassidy DB, Al Shakarchi J, McGrogan DG, Inston NG, Jones RG. Revisiting the risks of MRI with Gadolinium based contrast agents - review of literature and guidelines. *Insight Imaging*. 2015;6:553–558. doi:10.1007/s13244-015-0420-2
6. Errante Y, Cirimele V, Mallio CA, Di Lazzaro V, Zobel BB, Quattrocchi CC. Progressive increase of T1 signal intensity of the dentate nucleus on unenhanced magnetic resonance images is associated with cumulative doses of intravenously administered gadodiamide in patients with normal renal function, suggesting dechelation. *Invest Radiol*. 2014;49:685–690. doi:10.1097/rli.0000000000000072
7. Kanda T, Ishii K, Kawaguchi H, Kitajima K, Takenaka D. High signal intensity in the dentate nucleus and globus pallidus on unenhanced T1-weighted MR images: relationship with increasing cumulative dose of a gadolinium-based contrast material. *Radiology*. 2014;270:834–841. doi:10.1148/radiol.13131669
8. Fretellier N, Rasschaert M, Bocanegra J, et al. Safety and gadolinium distribution of the new high-relaxivity gadolinium chelate gadopiclenol in a rat model of severe renal failure. *Invest Radiol*. 2021;56:826–836. doi:10.1097/Rli.0000000000000793
9. Liu Z, Zhao ML, Wang H, et al. High relaxivity Gd3+-based organic nanoparticles for efficient magnetic resonance angiography. *J Nanobiotechnol*. 2022;2:20.
10. Liu SE, Jiang YX, Liu PC, et al. Single-Atom gadolinium nano-contrast agents with high stability for tumor T 1 magnetic resonance imaging. *Acs Nano*. 2023;17(9):8053–8063. doi:10.1021/acsnano.2c09664

11. Sadek H, Latif S, Collins R, Garry MG, Garry DJ. Use of ferumoxides for stem cell labeling. *Regener Med*. 2008;3(6):807–816. doi:10.2217/17460751.3.6.807
12. Ruggiero A, Guenoun J, Smit H, et al. In vivo MRI mapping of iron oxide-labeled stem cells transplanted in the heart. *Contrast Media Mol Imaging*. 2013;8(6):487–494. doi:10.1002/cmmi.1582
13. Saleh A, Schroeter M, Ringelstein A, et al. Iron oxide particle-enhanced MRI suggests variability of brain inflammation at early stages after ischemic stroke. *Stroke*. 2007;38(10):2733–2737. doi:10.1161/strokeaha.107.481788
14. Trivedi RA, Mallawarachi C, J-M. U-K-I, et al. Identifying inflamed carotid plaques using in vivo USPIO-enhanced MR imaging to label plaque macrophages. *Arterioscler Thromb Vasc Biol*. 2006;26(7):1601–1606. doi:10.1161/01.ATV.0000222920.59760.df
15. Hyafil F, Laissy JP, Mazighi M, et al. Ferumoxtran-10-enhanced MRI of the hypercholesterolemic rabbit aorta: relationship between signal loss and macrophage infiltration. *Arterioscler Thromb Vasc Biol*. 2006;26:176–181. doi:10.1161/01.ATV.0000194098.82677.57
16. Howarth SP, Tang TY, Trivedi R, et al. Utility of USPIO-enhanced MR imaging to identify inflammation and the fibrous cap: a comparison of symptomatic and asymptomatic individuals. *Eur. J. Radiol*. 2009;70:555–560. doi:10.1016/j.ejrad.2008.01.047
17. Degnan AJ, Patterson AJ, Tang TY, Howarth SP, Gillard JH. Evaluation of ultrasmall superparamagnetic iron oxide-enhanced MRI of carotid atherosclerosis to assess risk of cerebrovascular and cardiovascular events: follow-up of the ATHEROMA trial. *Cerebrovascular Dis*. 2012;34:169–173. doi:10.1159/000339984
18. Richards JM, Semple SI, MacGillivray TJ, et al. Abdominal aortic aneurysm growth predicted by uptake of ultrasmall superparamagnetic particles of iron oxide: a pilot study. *Circ Cardiovasc Imaging*. 2011;4:274–281. doi:10.1161/circimaging.110.959866
19. Sadat U, Howarth SP, Usman A, Tang TY, Graves MJ, Gillard JH. Sequential imaging of asymptomatic carotid atheroma using ultrasmall superparamagnetic iron oxide-enhanced magnetic resonance imaging: a feasibility study. *J Stroke Cerebrovascular Dis*. 2013;22:e271–276. doi:10.1016/j.jstrokecerebrovasdis.2012.06.015
20. Bernd H, De Kerviler E, Gaillard S, Bonnemain B. Safety and tolerability of ultrasmall superparamagnetic iron oxide contrast agent: comprehensive analysis of a clinical development program. *Invest Radiol*. 2009;44:336–342. doi:10.1097/RLI.0b013e3181a0068b
21. Elias A, Tsourkas A. Imaging circulating cells and lymphoid tissues with iron oxide nanoparticles. *Hematology*. 2009;720–726. doi:10.1182/asheducation-2009.1.720
22. Yilmaz A, Dengler MA, van der Kuip H, et al. Imaging of myocardial infarction using ultrasmall superparamagnetic iron oxide nanoparticles: a human study using a multi-parametric cardiovascular magnetic resonance imaging approach. *Eur Heart J*. 2013;34:462–475. doi:10.1093/eurheartj/ehs366
23. Alam SR, Shah AS, Richards J, et al. Ultrasmall superparamagnetic particles of iron oxide in patients with acute myocardial infarction: early clinical experience. *Circ Cardiovasc Imaging*. 2012;5:559–565. doi:10.1161/circimaging.112.974907
24. Bietenbeck M, Florian A, Sechtem U, Yilmaz A. The diagnostic value of iron oxide nanoparticles for imaging of myocardial inflammation--quo vadis? *J Cardiovasc Magn Reson*. 2015;17:54. doi:10.1186/s12968-015-0165-6
25. Stirrat CG, Alam SR, MacGillivray TJ, et al. Ferumoxytol-enhanced magnetic resonance imaging assessing inflammation after myocardial infarction. *Heart*. 2017;103:1528–1535. doi:10.1136/heartjnl-2016-311018
26. Usman A, Patterson AJ, Yuan J, et al. Ferumoxytol-enhanced three-dimensional magnetic resonance imaging of carotid atheroma- a feasibility and temporal dependence study. *Sci Rep*. 2020;10:1808. doi:10.1038/s41598-020-58708-x
27. Smits LP, Tiessens F, Zheng KH, Stroes ES, Nederveen AJ, Coolen BF. Evaluation of ultrasmall superparamagnetic iron-oxide (USPIO) enhanced MRI with ferumoxytol to quantify arterial wall inflammation. *Atherosclerosis*. 2017;263:211–218. doi:10.1016/j.atherosclerosis.2017.06.020
28. Brittenden J, Houston G, Lambie R, et al. Aortic wall inflammation predicts abdominal aortic aneurysm expansion, rupture, and need for surgical repair. *Circulation*. 2017;136:787–797. doi:10.1161/Circulationaha.117.028433
29. Unterweger H, Janko C, Folk T, et al. Comparative in vitro and in vivo evaluation of different iron oxide-based contrast agents to promote clinical translation in compliance with patient safety. *Int J Nanomed*. 2023 ;18: 2071–2086. doi:10.2147/IJN.S402320
30. Shokrollahi H. Contrast agents for MRI. *Mater Sci Eng C*. 2013;33:4485–4497. doi:10.1016/j.msec.2013.07.012
31. Unterweger H, Janko C, Schwarz M, et al. Non-immunogenic dextran-coated superparamagnetic iron oxide nanoparticles: a biocompatible, size-tunable contrast agent for magnetic resonance imaging. *Int j Nanomed*. 2017;12:5223–5238. doi:10.2147/ijn.s138108
32. Unterweger H, Dezsi L, Matuszak J, et al. Dextran-coated superparamagnetic iron oxide nanoparticles for magnetic resonance imaging: evaluation of size-dependent imaging properties, storage stability and safety. *Int j Nanomed*. 2018;13:1899–1915. doi:10.2147/Ijn.S156528
33. Moonen RPM, Coolen BE, Sluimer JC, Daemen MJAP, Strijkers GJ. Iron oxide nanoparticle uptake in mouse brachiocephalic artery atherosclerotic plaque quantified by T-2-mapping MRI. *Pharmaceutics*. 2021;13. doi:10.3390/pharmaceutics13020279
34. Ruehm SG, Corot C, Vogt P, Kolb S, Debatin JF. Magnetic resonance imaging of atherosclerotic plaque with ultrasmall superparamagnetic particles of iron oxide in hyperlipidemic rabbits. *Circulation*. 2001;103:415–422.
35. Kaneko C, Nitta N, Tsuchiya K, et al. MRI study of atherosclerotic plaque progression using ultrasmall superparamagnetic iron oxide in Watanabe heritable hyperlipidemic rabbits. *Br J Radiol*. 2015;3:88.
36. Durand E, Raynaud JS, Bruneval P, et al. Magnetic resonance imaging of ruptured plaques in the rabbit with ultrasmall superparamagnetic particles of iron oxide. *J Vasc Res*. 2007;44:119–128. doi:10.1159/000098484
37. Bai Q, Xiao Y, Hong H, et al. Scavenger receptor-targeted plaque delivery of microRNA-coated nanoparticles for alleviating atherosclerosis. *Proc Natl Acad Sci U S A*. 2022;119:e2201443119. doi:10.1073/pnas.2201443119
38. Nakamura M, Kosuge H, Oyane A, Kuroiwa K, Shimizu Y, Aonuma K. In vivostudy of iron oxide-calcium phosphate composite nanoparticles for delivery to atherosclerosis. *Nanotechnology*. 2021;32. doi:10.1088/1361-6528/ac007d
39. Yancy AD, Olzinski AR, Hu TC, et al. Differential uptake of ferumoxtran-10 and ferumoxytol, ultrasmall superparamagnetic iron oxide contrast agents in rabbit: critical determinants of atherosclerotic plaque labeling. *J Magn Reson Imaging*. 2005;21:432–442. doi:10.1002/jmri.20283
40. Matuszak J, Baumgartner J, Zaloga J, et al. Nanoparticles for intravascular applications: physicochemical characterization and cytotoxicity testing. *Nanomedicine*. 2016;11:597–616. doi:10.2217/nnm.15.216
41. Matuszak J, Zaloga J, Friedrich RP, et al. Endothelial biocompatibility and accumulation of SPION under flow conditions. *J Magn Magn Mater*. 2015;380:20–26.
42. Cicha I, Beronov K, Ramirez EL, et al. Shear stress preconditioning modulates endothelial susceptibility to circulating TNF-alpha and monocytic cell recruitment in a simplified model of arterial bifurcations. *Atherosclerosis*. 2009;207:93–102. doi:10.1016/j.atherosclerosis.2009.04.034

43. Diehl KH, Hull R, Morton D, et al. European federation of pharmaceutical industries a, european centre for the validation of alternative M. A good practice guide to the administration of substances and removal of blood, including routes and volumes. *J Appl Toxicol*. 2001;21:15–23. doi:10.1002/jat.727
44. Constantinides P, Booth J, Carlson G. Production of advanced cholesterol atherosclerosis in the rabbit. *Arch Pathol*. 1960;70:712–724.
45. Abela GS, Picon PD, Friedl SE, et al. Triggering of plaque disruption and arterial thrombosis in an atherosclerotic rabbit model. *Circulation*. 1995;91:776–784. doi:10.1161/01.Cir.91.3.776
46. Phinikaridou A, Hallock KJ, Qiao Y, Hamilton JA. A robust rabbit model of human atherosclerosis and atherothrombosis. *J Lipid Res*. 2009;50:787–797. doi:10.1194/jlr.M800460-JLR200
47. Matuszak J, Dorfler P, Lyer S, et al. Comparative analysis of nanosystems' effects on human endothelial and monocytic cell functions. *Nanotoxicology*. 2018;12:957–974. doi:10.1080/17435390.2018.1502375
48. Matuszak J, Lutz B, Sekita A, et al. Drug delivery to atherosclerotic plaques using superparamagnetic iron oxide nanoparticles. *Int J Nanomed*. 2018;13:8443–8460. doi:10.2147/IJN.S179273
49. Chao Y, Makale M, Karmali PP, et al. Recognition of dextran-superparamagnetic iron oxide nanoparticle conjugates (Feridex) via macrophage scavenger receptor charged domains. *Bioconjug Chem*. 2012;23:1003–1009. doi:10.1021/bc200685a
50. Tang TY, Howarth SP, Miller SR, et al. Comparison of the inflammatory burden of truly asymptomatic carotid atheroma with atherosclerotic plaques contralateral to symptomatic carotid stenosis: an ultra small superparamagnetic iron oxide enhanced magnetic resonance study. *J Neurol Neurosurg*. 2007;78:1337–1343. doi:10.1136/jnnp.2007.118901
51. Tang TY, Howarth SP, Miller SR, et al. Comparison of the inflammatory burden of truly asymptomatic carotid atheroma with atherosclerotic plaques in patients with asymptomatic carotid stenosis undergoing coronary artery bypass grafting: an ultrasmall superparamagnetic iron oxide enhanced magnetic resonance study. *Eur J Vasc Endovascular Surg*. 2008;35:392–398. doi:10.1016/j.ejvs.2007.10.019
52. Knobloch G, Colgan T, Wiens CN, et al. Relaxivity of Ferumoxytol at 1.5 T and 3.0 T. *Invest Radiol*. 2018;53:257–263. doi:10.1097/RLI.0000000000000434
53. Weinstein JS, Varallyay CG, Dosa E, et al. Superparamagnetic iron oxide nanoparticles: diagnostic magnetic resonance imaging and potential therapeutic applications in neurooncology and central nervous system inflammatory pathologies, a review. *J Cereb Blood Flow Metab*. 2010;30:15–35. doi:10.1038/jcbfm.2009.192
54. van Hoof RHM, Schreuder F, Nelemans P, et al. Ischemic stroke patients demonstrate increased carotid plaque microvasculature compared to (ocular) transient ischemic attack patients. *Cerebrovascular Dis*. 2017;44:297–303. doi:10.1159/000481146
55. Cicha I, Worner A, Urschel K, et al. Carotid plaque vulnerability: a positive feedback between hemodynamic and biochemical mechanisms. *Stroke*. 2011;42:3502–3510. doi:10.1161/STROKEAHA.111.627265
56. Banda NK, Mehta G, Chao Y, et al. Mechanisms of complement activation by dextran-coated superparamagnetic iron oxide (SPIO) nanoworms in mouse versus human serum. *Part Fib Toxicol*. 2014;11:1–10. doi:10.1186/s12989-014-0064-2
57. Wang G, Chen F, Banda NK, et al. Activation of human complement system by dextran-coated iron oxide nanoparticles is not affected by dextran/Fe ratio, hydroxyl modifications, and crosslinking. *Front Immunol*. 2016;7:418. doi:10.3389/fimmu.2016.00418
58. Szebeni J, Fishbane S, Hedenus M, et al. Hypersensitivity to intravenous iron: classification, terminology, mechanisms and management. *Br. J. Pharmacol.* 2015;172:5025–5036. doi:10.1111/bph.13268
59. Smits LP, Coolen BF, Panno MD, et al. Noninvasive differentiation between hepatic steatosis and steatohepatitis with MR imaging enhanced with USPIOs in patients with nonalcoholic fatty liver disease: a proof-of-concept study. *Radiology*. 2016;278:782–791. doi:10.1148/radiol.2015150952
60. Department of Health and Human Services FaDA. *Guidance for Industry: Estimating the Maximum Safe Starting Dose in Initial Clinical Trials for Therapeutics in Adult Healthy Volunteers*. U.S: Department of Health and Human Services FaDA; 2005.